



Research paper

Development of a modular approach for photovoltaic module lifetime and reliability estimation

Suraj Ravindrababu ^{a,b}, Ingrid Hädrich ^a, Ulrich W. Paetzold ^b, Paul Gebhardt ^{a,*}

^a Fraunhofer Institute for Solar Energy Systems ISE, Heidenhofstrasse 2, Freiburg, 79110, Baden-Württemberg, Germany

^b Karlsruhe Institute of Technology, Light Technology Institute (LTI), Engesserstrasse 13, Karlsruhe, 76131, Baden-Württemberg, Germany



ARTICLE INFO

Dataset link: <https://gitlab.cc-asp.fraunhofer.de/maple/maple>

Keywords:

Degradation
Predictive models
Empirical and physics-based models
Modular computational models
Photovoltaics

ABSTRACT

Assessing the impact of environmental stresses on the performance of photovoltaic (PV) modules by predictive modeling is crucial for evaluating their sustainability and economic viability. While various data-driven and analytical models for PV degradation have been reported, no prior efforts have integrated these approaches for a more robust prediction. This article presents the development of an open-sourced holistic degradation modeling framework, called MAPLE, which integrates three distinct modeling approaches identified from the literature: coupled failure modeling (CFM), mode-specific modeling (MSM), and multi-scale failure modeling (MFM). In this work, CFM is extended to modern cell technologies by fitting field degradation data from literature for modules with heterojunction cells. MSM employs selected analytical models that represent the failure of modules due to specific degradation modes, with a multiplicative coupling method to combine the effects of multiple degradation modes on performance. Additionally, the concept of equivalent time is implemented to extrapolate indoor models for outdoor predictions. The MFM approach introduces a novel first principles method for degradation modeling by aggregating degradation across varying length scales, exemplified by simulating overall power loss of a module from hail damage. MFM simulation results are validated against a hail-impacted module, showing a deviation of 5.75%. The advantages and limitations of the three modeling approaches are discussed, along with future research directions to enhance the modeling approaches within MAPLE.

1. Introduction

The reliability of photovoltaic (PV) modules is a critical factor for the sustainability and economic viability of PV installations (Kaaya et al., 2020). While a lifespan of over 20 years and a linear degradation rate of approximately 0.5% per year are often assumed, real-life degradation can vary significantly depending on specific environmental conditions (Theristis et al., 2023). Degradation modeling is a form of predictive analytics to determine evolution of PV module output due to degrading material and components exposed to environmental stressors. Lindig et al. classify degradation modeling approaches as data-driven and analytical (Lindig et al., 2018). They state that data-driven models are empirical models fitted to field degradation datasets, whereas analytical models are traditional frameworks based on physical and chemical theories derived from rigorous experimentation, requiring a more complex methodology and greater resource investment for development (Jang et al., 2021). However, it is essential to thoroughly investigate the circumstances of the implementation of the two modeling approaches within the photovoltaic (PV) community

to attain a comprehensive understanding of the advantages and limitations of both analytical and data-driven modeling methods, particularly regarding their adaptability in assessing the reliability of continuously evolving module materials, design and lamination processes (Öz et al., 2025).

Degradation analysis can be performed at various time and length scales and can be evaluated at the system, module, or cell level. At the system level, apart from module degradation, the performance loss effect encompasses loss due to array maximum power point (MPP) mismatch, resistance losses due to increasing cable and connector resistances, and inverter losses due to noise and degradation, among others. Approaches to modeling degradation at this level have primarily been data-driven (Jordan et al., 2017b). These approaches analyze PV production data collected over several years to determine the degradation or performance loss rates (PLR) for specific module and system configuration (Deceglie et al., 2018). Most importantly, several modeling frameworks, such as RdTools, PVLife (Mikofski et al., 2012), are available to measure overall degradation through the statistical analysis

* Corresponding author.

E-mail address: paul.gebhardt@ise.fraunhofer.de (P. Gebhardt).

<https://doi.org/10.1016/j.egy.2026.109323>

Received 16 July 2025; Received in revised form 5 March 2026; Accepted 11 April 2026

Available online 25 April 2026

2352-4847/© 2026 The Authors. Published by Elsevier Ltd. This is an open access article under the CC BY license (<http://creativecommons.org/licenses/by/4.0/>).

of PV system output data. Most of these frameworks assume a linear degradation rate and the approach makes it impossible to differentiate the contributions from the degradation modes acting at the module and cell levels to the overall degradation.

Degradation at the module and cell levels results primarily from material deterioration over time as a result of environmental stresses. Some common degradation modes at the module level include encapsulant discoloration, cell metallization corrosion (Hacke et al., 2010), delamination (Aghaei et al., 2022), glass corrosion and potential-induced degradation (PID) (Pingel et al., 2010). At the cell level, cell cracking (Eitner et al., 2009), ultraviolet-induced degradation (UV ID) (Sinha et al., 2023), and light and elevated temperature-induced degradation (LeTID) (Fokuhl et al., 2021) are some modes that directly affect the diode behavior. Degradation models at the cell and module levels are primarily analytical in nature. These models are based on well-established life-stress relationships, such as the Arrhenius model, Peck's model (Peck, 1986a), and Norris-Landzberg model (Norris and Landzberg, 1969). These models relate the rate of degradation of a material (e.g., transmittance) or module parameter (e.g., short-circuit current) to environmental variables (such as temperature, relative humidity, and ultraviolet dose). The model parameters are calibrated using indoor accelerated test data from modules subjected to constant test conditions in a controlled environment. These analytical models are sometimes referred to as physics-of-failure (PoF) models, as they encompass the physical and chemical mechanisms underlying the degradation modes.

The initial example of the development of PoF models for photovoltaic (PV) modules is found in the seminal works of R.E. Thomas and G.B. Gaines (Gaines et al., 1977). R.E. Thomas emphasizes that deriving physics-based models is challenging when a system is subjected to multiple geographical and non-geographical factors simultaneously (Thomas and Gaines, 1979). The effect of simultaneous stresses may initiate several degradation mechanisms, which may or may not evolve independently. Individual PoFs are therefore rarely linked in degradation modeling making it difficult to compute the total degradation in field-installed PV modules (Chiacchio et al., 2019). Unlike tools available for analysis at the system level, a framework is unavailable in literature to integrate and work with PoFs' for reliability assessment of PV modules.

It is futile to argue which degradation modeling approach is generally the best for predicting field lifetime and reliability. Kaaya et al. advocate for a generalized approach comprising four key facets: correlating indoor accelerated test data with outdoor conditions, predicting the degradation of novel materials, assessing the impact of new module designs on performance, and evaluating the influence of environmental parameters (Kaaya et al., 2023). The ability of a degradation modeling approach to integrate PoFs' for field prediction is, therefore, vital. Accelerated tests are conducted to obtain reliability information quickly and this data should be utilized for degradation modeling (Escobar and Meeker, 2006). Springer et al. calls for a holistic degradation modeling approach that can model multiple degradation mechanisms based on PoFs' and data-driven models, while also being interchangeable across different modeling approaches (Springer et al., 2023). Interchangeability between modeling approaches is crucial when gaps in prediction capability arise within the framework. In such scenarios, a purely data-driven approach might estimate the overall degradation of a module at a given location in the absence of applicable PoFs'. Selecting data-driven or PoFs' to predict evolution of PV output also depends on the requirements of the stakeholders. For instance, power plant owners and technology insurers might be more interested in the absolute lifetime of a module at a specific geographic location, which can be determined using data-driven or stochastic modeling techniques (Charki et al., 2013). An approximation of the yearly degradation rate can be obtained when field degradation data or performance time-series data are available (Jordan et al., 2017c, 2016). However, for energy service providers, information on daily yield could be important. For example,

when modules are affected by potential-induced degradation (PID), modeling both the degradation and regeneration processes (Pingel et al., 2012) becomes critical for these types of stakeholders and is best accomplished using a PoF model. Therefore, a robust degradation modeling framework must enable the computation of reliability through both data-driven and PoF models.

The importance of simulating degradation at different length scales is reinforced by the article by Jordan et al. (2022). They also emphasize the need for modularity, meaning the ability to calibrate existing physics of failure (PoFs) or other new models as materials and cell technologies evolve. The data-driven and PoFs discussed previously assume that the degradation mode is homogenized within the module space. However, some degradation modes are not influenced by module size (e.g., solder joint fatigue (Bosco and Silverman, 2021)) or occur locally within the PV module (e.g., ECA interconnection failures (Springer et al., 2021), hot spots (Hartley, 2021), and cell cracks due to hail impact (Gupta et al., 2022)). A review of multi-scale techniques applied to PV technology describes the different length scales of interest (Hamed et al., 2018). Modeling degradation at the atomic scale is impractical, as the development of materials occurs at a rapid pace, making it difficult to model the degradation physics of all material property combinations. However, at the cell level, the effects of various stresses on cell electrical characteristics can be formulated as PoFs through experiments. Although degradation models that map the evolution of local failures, such as cell cracks or interconnection failures, as a function of environmental variables are scarce, it is crucial for a degradation modeling framework to incorporate cell-level effects to accurately calculate module lifetime and reliability.

Based on the arguments presented above, it is clear that integrating the three modeling approaches, which include data-driven models, analytical or physics of failure (PoF) models, and a multi-scale approach, into a simple and logical framework is beneficial. In this article, we present the development of a degradation modeling framework called MAPLE, which stands for Modular Approach for Photovoltaic Module Lifetime and Reliability Estimation. The modular framework integrates the different modeling approaches and combines them with meteorological data for robust degradation assessment of PV modules. MAPLE is developed by identifying, reviewing and implementing important data-driven and analytical models available in literature. Although MAPLE uses models available in literature, some important contributions in this work involve:

- The classification of degradation modeling approaches into three types of modeling strategies:
 - Coupled Failure Modeling (CFM): A purely data-driven modeling strategy which uses field degradation data for degradation prediction.
 - Mode Specific Modeling (MSM): A degradation modeling strategy which is based on PoFs'.
 - Multi-Scale Failure Modeling (MFM): This modeling strategy computes module-level degradation by combining degradation effects happening at the cell-level by providing a handle over individual cell parameter evolution through time. Degradation modes which are studied at cell-level through mini-modules or cell samples can be incorporated into this approach.
- Within MAPLE, the CFM approach is extended to predict the field degradation of heterojunction (HJT) modules through a non-linear regression analysis on field performance data. The CFM model for HJT is validated by comparing the performance loss rates (PLRs) for HJT modules available in the literature.
- Within the MSM module, MAPLE provides methods to combine two or more degradation modes, whether independent or dependent, to calculate the overall degradation in power. Although validation is challenging due to the unavailability of outdoor

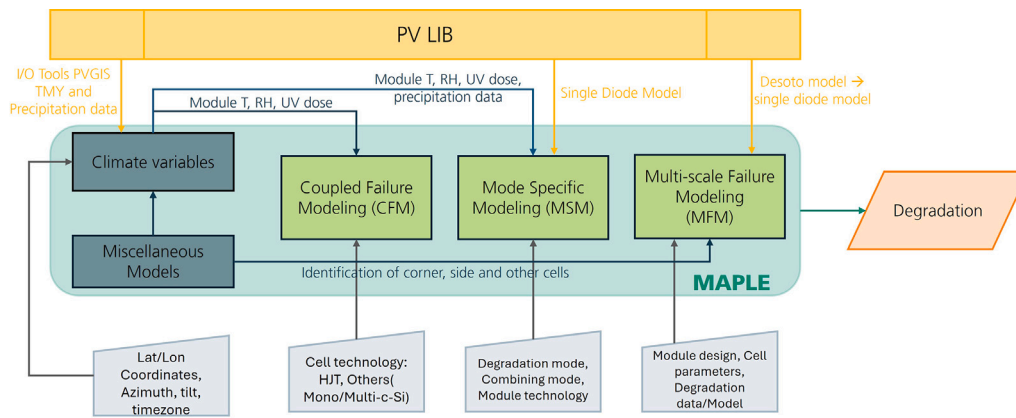


Fig. 1. The MAPLE framework.

data for the modules used to calibrate these PoFs, which were developed based on indoor accelerated test data, the framework aims to enhance the understanding of degradation mechanisms and their influence on the overall output power.

- Within the MSM module, an important concept called equivalent time is proposed and its importance in extrapolating PoFs' based on indoor accelerated test data to field predictions is elucidated.
- Within the MFM modules, although the availability of degradation models is scarce, the functionality of aggregating local degradation in module space is illustrated by studying cell cracks due to hail impacts on a standard commercial PV module. The overall degradation in power predicted by MAPLE is validated through indoor hail impact experiments.

MAPLE uses the PVlib Python toolbox to work with climate data (Jensen et al., 2023a) and to compute the electrical parameters of cells and modules (Holmgren et al., 2018). Developing the MAPLE Python library represents a significant step forward in providing an open-sourced, modular tool for researchers, engineers and industry professionals alike. The library aims to unify different methodologies into a single platform, simplifying the process of degradation prediction and enhancing model comparability. The library aims to make degradation modeling more accessible, efficient and motivates design of accelerated tests for degradation modeling.

The article is structured as follows: Section 2 illustrates the structure of the MAPLE framework. Section 3 elaborates on the different parts of MAPLE, elaborating the classification of degradation modeling strategies, including the mathematical descriptions of the models for each category within MAPLE. Section 4 shows the implementation of MAPLE and discusses the merits and demerits of the different modeling strategies. This section also exemplifies important concepts within each degradation modeling strategy. Finally, Section 5 summarizes the work presented in the article along with potential areas for further enhancement of the MAPLE framework.

2. MAPLE structure

The structure of the MAPLE framework is shown in Fig. 1. MAPLE comprises five modules: climate data, miscellaneous models, CFM, MSM, and MFM. These modules are segregated to ensure modularity and comparability. New models within each modeling strategy, or to compute climatic stresses such as module temperature or irradiation, can be implemented with minimal code changes. Furthermore, this segregation enhances code readability and aids in understanding the workflow for computing degradation using a modeling strategy.

To use MAPLE effectively, users must identify the appropriate degradation strategy for their needs. They also need location parameters (latitude and longitude), cell technology, and module design data. The

choice between MSM, CFM, or MFM strategies will depend on user requirements, which will be elaborated in the following sections.

In brief:

- CFM predicts absolute performance loss for a specific cell technology.
- MSM is applied when users have additional data on module technology and material degradation, allowing for a combination of degradation behaviors.
- MFM is beneficial when detailed degradation evolution information is available, such as degradation changes with field variables or the distribution or concentration of degradation within a module.

The climate data processing module has functions to obtain climate data from PVGIS using PVLib's i/o tools (Jensen et al., 2023b). The climate module comprises of functions to obtain typical meteorological data (TMY), which is used for calculating the climatic stresses in most of the degradation models inside MAPLE. Some strategies, for example CFM, have unique calculations for estimating module temperature or UV dose. Such calculations are programmed to be done within the climate module. The output of the climate module will then be the climatic stresses, computed as stated in the parent article from where the model is derived, which could then be directly used for calculation.

Models for calculating the module temperature, UV dose and the algorithm to segregate corner and side cells for MFM strategy is implemented within the miscellaneous models module.

MSM uses the single diode model inside PV-Lib to compute the points of the IV curve (Jain and Kapoor, 2004; Wenham et al., 2013). Similarly, MFM uses the De Soto model to compute the five parameters required for the single diode model (De Soto et al., 2006). Therefore, for MSM, the degradation of properties at the module level is computed while for MFM, the cell temperature, irradiance and other diode properties could be given as input. This improves degradation computation while using MFM, which is discussed later.

MFM alone includes two sets of codes for simulating modules with substrings connected in series or parallel. The linking of climate and miscellaneous models to the codes is not currently feasible, as MFM requires the user to input the degradation evolution of each of the cells in the module. This is the reason that we enable the inclusion of the IV characteristics of each cell using Pandas dataframe as mentioned above. This aspect will be enhanced in the future as more models are developed, focusing on a bottom-up approach to degradation modeling.

3. Classification of degradation modeling approaches

This section elaborates on the different approaches towards degradation modeling of PV modules and their implementation within MAPLE. Apart from degradation approaches mentioned in Section 1,

stochastic/bayesian processes such as the Wiener process, Gamma process, and inverse Gaussian process are commonly used to determine the remaining useful life (RUL) of PV modules (Charki et al., 2013). Stochastic processes treat model parameters as random variables and assign a probability density function (p.d.f.), known as a prior or belief. These parameters are then updated based on available degradation data (Wen et al., 2018). Such data-driven approaches, hence, produce several degradation paths based upon the variance of the model parameters. Consequently, we can estimate the RUL and it is variance accurately, provided a large amount of degradation data is available. For this, field degradation data is required to calibrate the model parameters or the PLR of the module technology should be a known priori. The continuous introduction of new cell technologies and materials complicates the prediction of their performance reliability. Furthermore, combining different degradation pathways, even if the corresponding mechanisms are known, is quite challenging with stochastic processes.

Since the stochastic approach provides similar challenges as the data-driven approach, this method is currently not incorporated into the MAPLE framework.

In this section, we differentiate and elucidate each of the modeling strategies working within MAPLE.

3.1. Coupled failure modeling (CFM)

CFMs compile accelerated life-stress models to describe the degradation rate due to various climatic stressors. The initial ideas for the CFM modeling approach is laid in a report by Gaines G.B. Gaines et al. (1979a). A practical implementation of the modeling strategy is provided by Kaaya et al. (2019). In this implementation, three main degradation reactions are assumed to dominate, mainly hydrolysis, photo-degradation and thermo-mechanical stresses due to the temperature cycling effect. Hydrolysis driven degradation is driven mainly by temperature and relative humidity and is described using the Peck's model (Peck, 1986b). The photo-degradation happening due to ultraviolet (UV) dose, temperature and relative humidity is represented using a combination of Peck's model and power law. Finally, the thermo-mechanical degradation due to temperature cycling is computed using Norris-Landzberg model. The CFM model inside MAPLE is based on Kaaya et al. implementation and is given as follows:

$$\text{Hydrolysis} : k_H = A_1 * rh_{eff}^{n_1} * \exp\left(\frac{-E_{a1}}{k * T_m}\right) \quad (1)$$

$$\text{Photo - Degradation} : k_{pH} = A_2 * UV_{dose}^{n_2} * (1 + rh_{eff}^{n_1}) * \exp\left(\frac{-E_{a2}}{k * T_m}\right) \quad (2)$$

$$\text{Temperature - cycling} : k_{TC} = A_3 * (\Delta T)^{n_3} * C_n * \exp\left(\frac{-E_{a3}}{k * T_{max}}\right) \quad (3)$$

where k_H , k_{pH} and k_{TC} are the calculated degradation reaction rate due to different the stress combinations (%/year), k is the Boltzmann constant in eV/K (8.62×10^{-5}). A_1 , A_2 and A_3 represent the positive pre-exponent factors (%/year), T_m is the module temperature (K) calculated using Faiman model (Faiman, 2008), n_1 , n_2 and n_3 represent the power exponents of relative humidity, UV dose and temperature cycle, rh_{eff} ($\frac{RH\%}{100}$) is the effective module relative humidity calculated as shown in Koehl et al. (2012), and E_{a1} , E_{a2} and E_{a3} are the activation energies (in eV). In Eq. (3), $\Delta T = T_{max}^{mod} - T_{min}^{mod}$ ($^{\circ}$ C) is computed as the difference of the upper (98th percentile) and lower percentile (2.5th percentile) of a module temperature distribution. This avoids any measurement errors in the climate data. UV_{dose} (kWh/m²) is calculated using Wald's model which includes the clearness index and plane of array irradiance (E_{POA}) to estimate the total UV irradiance from its components (Wald, 2018). The individual reaction rates are coupled using an equation:

$$k_T = A_N * \prod_{i=1}^m (1 + k_i) - 1 \quad (4)$$

Table 1

CFM parameters for Mono-Si modules (Kaaya et al., 2019).

Model	A_i	n_i	E_{a_i}
Hydrolysis:	4.91e7	1.90	0.74
Photo-Degradation:	71.83	0.63	0.45
Thermo-Mechanical:	2.04	2.24	0.43

where the subscript $i=1,2, \dots, m$ denotes the number of degradation mechanisms included in the CFM formulation, and A_N (%/year) is the pre-exponent factor. Lastly, the overall degradation rate (k_T (%/year)) is brought together to predict the evolution of power through the exponential functional form:

$$P_{norm}(t) = 1 - \exp\left(-\left(\frac{B}{(k_T * time)}\right)^\mu\right) \quad (5)$$

where B is a model parameter and μ is a shape parameter which makes Eq. (5) quite versatile to accommodate different degradation path shape. Kaaya et al. determine the CFM model parameters by calibrating the model to outdoor performance data. It is also highlighted that the determined model parameters are applicable only to mono-crystalline silicon (mono-Si) modules, and they are presented in Table 1.

Inside MAPLE, CFM is extended to work for heterojunction (HJT) and polycrystalline (poly-Si) modules by calibrating the model using field performance data available in literature. During the non-linear least squares fitting of the data to the CFM model, multiple numerical solutions can satisfy the models. For determining the best solution, Kaaya et al. recommends calibrating the model using atleast data from two different locations for a module with similar technology (Kaaya et al., 2021). The model parameters are determined by fitting the CFM formulation to field degradation data available at 11 (for HJT) and 7 (for pSi) different locations around the world (Carigiet et al., 2021; Luo et al., 2018; Raghuraman et al., 2006; Limmanee et al., 2016; Makrides et al., 2014; Sharma et al., 2014; Schweiger et al., 2017; Ishii et al., 2018; Jordan et al., 2017a). Degradation data is digitized from literature using a plot-digitizer whose validity and reliability is proven (Aydin and Yassikaya, 2022).

For model calibration, we use prior-information available for each of the model parameters. For example, we know pre-exponential factors (A_1 , A_2 and A_3) cannot be negative as they represents the frequency of collision between reactant molecules at a given concentration. Also, activation energies (E_{a1} , E_{a2} and E_{a3}) represents an energy barrier that has to be overcome by the reactants to produce degradation products. Therefore, these parameters are set to be always positive, but can take values up to infinity, when fitting to data.

3.2. Mode specific modeling (MSM)

MSMs focus on degradation models derived from accelerated experiments on full-scale PV modules and material degradation data. The focus of the MSM implementation is two fold. Firstly, is to use the degradation model formulated using accelerated degradation tests to predict field results. Secondly, to formulate a simplistic approach to combine degradation effects of each of these models.

In MAPLE, MSM models are designed to compute normalized power P_{norm} given by:

$$P_{norm} = \frac{P(t)}{P_0} \quad (6)$$

$$\text{Degradation, } D(\%) = \left[1 - \frac{P(t)}{P_0}\right] * 100 \quad (7)$$

$P(t)$ (W) represents the absolute power value at time t , while P_0 (W) denotes the initial power before degradation. The combined normalized power P_{norm}^C is computed as:

$$P_{norm}^{independent} = \prod_{i=1}^m P_{norm}^i \quad (8)$$

where $i = 1...m$ denotes m independent degradation modes. For dependent degradation modes, where the initiation and progression of D_1 depend on D_2 , the degradation in power cannot be approximated as the product of the normalized powers of D_1 and D_2 individually (Wang and Coit, 2004). For calculating the effect of dependent degradation modes, a multiplicative models of degradation as proposed by Zagorowska et al. is formulated (Zagorowska et al., 2020), which resembles conditional probabilities in statistics. Dependent degradation modes can be combined through Eq. (9) as:

$$P_{norm}^{dependent} = (1 - (k^A * D^A)) * (1 - (k^B * D^B)), \text{ where } 0 \leq k^{A,B} \leq \infty \quad (9)$$

If $k^{A,B}=1$, then A and B are two independent degradation events as it gets reduced to Eq. (8). If $0 < k_A < 1$ in the presence of B, then the degradation effect is alleviated. However, if $1 \leq k_A \leq \infty$ the presence of mode B exacerbates the degradation effect due to mode A. k_A, k_B are scaling factors whose value should be experimentally determined.

For the definition of the parameters of the models used in MSM, please refer to the supplementary information provided with this article.

3.2.1. Corrosion: Damp-heat degradation model

Corrosion is one of the critical end-of-life degradation modes occurring in PV modules. Corrosion is generally related to the formation of acetic acid due to the hydrolysis of ethylene vinyl acetate (EVA) encapsulant which affects the cell passivation, metallization and module interconnection (Fairbrother et al., 2022). The damp-heat (DH) test is the accelerated test chosen to study corrosion (Kyranaki et al., 2022). A comprehensive degradation model for the evolution of power and series resistance due to corrosion is provided by Braisaz et al. (2014).

$$P_{indoor}(t, T, RH) = \frac{1 + e^{-B}}{1 + e^{R_d^P(T, RH) * t - B}} \quad (10)$$

$$R_s = R_{s,initial} + \exp(R_d^S * t - B) \quad (11)$$

Eqs. (9), (10) are fitted to DH degradation tests conducted at 85 °C/85%RH, 95 °C/85%RH, and 95 °C/58%RH to obtain the values of R_d^P, R_d^S, B . They are related to the module temperature (T) and relative humidity (RH) using the Peck's model as:

$$R_d^{P,S}, B = A * (RH)^n * \exp\left(\frac{-E_a}{k_b * T}\right) \quad (12)$$

Eq. (9). describes the power to follow sigmoidal path of degradation. While implementing it outdoors, unlike accelerated tests, the T and RH vary in every time step. For Eq. (8). to hold true, the time increment for every degradation mode should be equal to the mode that has the smallest time step. To realize this, the computation of an equivalent time step is critical and the outdoor degradation path is not sigmoidal, as in Eq. (9), but rather a complex combination of several sigmoids as T and RH changes in every time step. Equivalent time can be defined as the time increment to be added to the time step for a quantity to degrade as much as in the last time step for the covariates in the current time step. If P_i, C_i denotes the power and covariates (T, RH, etc.) at time i and Δt denotes the step size, then the equivalent time is sum of the time required for the power to reach value $P_{i-\Delta t}$ at time i (C_i) and the step size. The importance of calculating the equivalent time is explained in the next section. The equation for computing equivalent time is given as:

$$\text{Powermodel : Equivalent - time, } t_{eq} = \frac{B(t) + \log\left(\frac{1+e^{-B}}{P_{norm}(t-\Delta t)} - 1\right)}{R_d(t)} \quad (13)$$

$$R_s \text{ model : Equivalent - time, } t_{eq} = \frac{\log(P_{norm}(t-\Delta t) - 1) + B(t)}{R_d(t)} \quad (14)$$

3.2.2. UV-induced degradation in PERC and HJT modules

UV induced degradation in p-type passivated emitter and rear cells (PERC) due to the degradation of silicon nitride passivation (SiN) layer is reported by Witteck et al. (2017). The degradation in power (P_{mpp}) is reported for single-cell modules due to UV exposure up to 500 kWh/m² for encapsulants with UV blocking and transmitting EVA encapsulants. Furthermore, two groups of modules with different refractive index of SiN coatings were exposed to UV irradiation. The degradation in power is modeled by a reduction in the open-circuit voltage (V_{oc}) due to an increased recombination of the cell. The equation is given as:

$$V_{oc} = \frac{kT}{q} \ln\left(\frac{I_{sc}}{J_{0i} + q \frac{n_i^2}{n_s} v_{th} \sigma_p (N_T - N_{P0}) \exp[-\sigma_{UV}(\lambda) * \phi_b t]} + 1\right) \quad (15)$$

The UV induced degradation in power of commercial HJT solar modules is modeled by Ren et al. (2024). Here she uses change point regression to differentiate the degradation before and after the depletion of the UV-sensitive reactants in the passivation layer. The model and parameters are valid for two modules with UV cut and UV pass encapsulants. The change-point model is simplified to directly predict the normalized power. The model form and the change point location is preserved to ensure the capability of the model as reported.

$$P_{norm} = a_1 - \frac{b_1}{1 + \exp(c_1 - (d_1 * UV_{dose}))} \quad (16)$$

a_1, b_1, c_1 and d_1 are empirical parameters which vary for UV pass and UV cut modules. The change-point is assigned at 80kWh/m² and 120 kWh/m² for UV cut and UV pass modules.

3.2.3. Encapsulant discoloration models

The degradation in power due to encapsulant discoloration in EVA back-sheet modules is described by Sinha et al. (2018). The article recommends the use of a modified Arrhenius model to describe the degradation rate of short-circuit current due to loss in transmittance caused by the discoloration of the encapsulants. The model was chosen since the activation energy describing the degradation is within the range of 0.27 to 0.46 eV. Sinha et al. recommends the value of 0.31 eV for the activation energy as it was comparable to their outdoor field testing results. The modified Arrhenius model is described as:

$$r_d^{I_{sc}}(T, UV) = A * \exp\left(\frac{-E_a}{kT}\right) * (UV)^n \quad (17)$$

The degradation in glass-glass laminated EVA encapsulates is described using the experimental data published by Miller et al. (2015). The article describes a linear degradation in representative solar weighted transmittance ($\tau_{rs,w}$) of EVA glass-glass modules. The influence of temperature in $\tau_{rs,w}$ is expressed by the Arrhenius relationship as:

$$r_d^{\tau_{rs,w}}(T) = A * \exp\left(\frac{-E_a}{kT}\right) \quad (18)$$

The article recommends an activation energy value of 60 kJ/mol (\approx 0.6 eV). By fitting the data available in the article, the model in MAPLE works with an activation energy of 0.62 eV.

3.2.4. Potential induced degradation (PID) model :degradation and regeneration

The degradation and regeneration of module power due to PID-s is modeled as described by Annigoni (2018). Annigoni's PID model is chosen as it clearly lays down the models driving daytime degradation, regeneration and nighttime regeneration along with the model parameters. The daytime regeneration model is based on Hacke et al. degradation model (Hacke et al., 2015). The regeneration model for daytime and nighttime degradation is driven by an exponential acceleration model (Schnepf et al., 2015) as shown below:

- **Daytime Degradation:** Degradation during the daytime is initiated when the relative humidity (RH) > 40% and the precipitation is high (rain) or if the module temperature (T_{mod}) is less than the dew point temperature ($T_{dew\ point}$) + 10 °C.

$$P_{max}(t) = P_{ini} \cdot \left(1 - A \cdot V \cdot RH^b \cdot \exp\left(\frac{-E_a}{kT}\right) \cdot t^2\right) \quad (19)$$

P_{ini} is the power at the start of the degradation process.

- **Daytime Regeneration:** Regeneration during the daytime is initiated in dry conditions, i.e., if the RH < 40%.

$$RR(t) = \lambda \left[1 - \exp\left(-\frac{t}{\tau}\right)\right]^\beta \quad (20)$$

$$\tau = 800 \text{ h}, \beta = 0.5, \text{ and } \lambda = \begin{cases} 1 & \text{if } \frac{P_{min}}{P_{ini}} > 0.5 \\ 2 \cdot \frac{P_{min}}{P_{ini}} & \text{otherwise} \end{cases}$$

- **Nighttime Regeneration:** Regeneration in the nighttime is identified by the timestamp in the typical meteorological data (TMY) handled by MAPLE.

$$RR(t) = 1 - \exp\left[-\left(\frac{t}{\tau(T)}\right)^\beta\right] \quad (21)$$

where $\beta = 0.55$ and

$$\tau(T) = \tau(T_{ref}) \cdot \exp\left(\frac{-E_a}{k} \cdot \left(\frac{1}{T} - \frac{1}{T_{ref}}\right)\right)$$

with $E_a(\tau) = 0.52 \text{ eV}$, $T_{ref} = 30 + 273.15 \text{ K}$.

3.3. Multi-scale failure modeling (MFM)

The multi-scale failure modeling library (MFM) enables to control the electrical characteristics of each cell in a module. To enable this, MAPLE numbers each cell based on the number of substrings/arrays and the total number of cells present inside the module. A function in MAPLE groups the cells automatically according to their location and classifies them to be either corner cells or side cells. A typical arrangement of a module with 5 substrings and 60 cells is shown in Fig. 2. This approach varies the properties of cells based on their location. For instance, moisture ingress leads to cell degradation that correlates with moisture concentration within the cells (Gnocchi et al., 2024). However, the concentration would be different in the corner and side cells, with the corner cells at a higher concentration. In the presence of a model that models the degradation as a function of the moisture concentration, the model could then be easily implemented.

MAPLE calculates the IV curve of each cell and stores it as a Pandas data-frame (Wes McKinney, 2010). The degradation model, in the above example, could be formulated to calculate the IV curves for each cell at a given time step and store them as a Pandas data-frame. This can then be given as an input into MAPLE by simply mentioning the data-frame name along with the number. For example, the IV curves of cell 1 could be simply given into the code as (df_1, df is the dataframe name with 2 columns I and V).

MAPLE enables the connection between the arrays/substrings in a module to be connected in parallel or in series. This could also help in determining the effects of module design on degradation. Probabilistic description of degradation, stated in the introduction, and uncertainty quantification is also possible through this scheme. To combine cells/substrings connected in series, the voltage at similar current values are added together. Similarly, for a parallel connection, the current is added at similar voltage positions through interpolation.

$$\text{Cells/Substrings connected in series: } v_+ = v^c \quad (22)$$

$$\text{Cells/Substrings connected in parallel: } i_+ = i^c \quad (23)$$

$c=1,\dots,n$, where n is the total number of cells or substrings being connected in parallel or in series.

Models designed to work along with MFM that can be directly integrated into our computation are currently unavailable. Therefore, in this article the impact of cell cracks on the degradation in power is shown as an example.

4. Results and discussion

4.1. CFM: a workflow for quick degradation prediction

4.1.1. Validation of CFM implementation for HJT modules

Arruti et al. published an article on the long term performance and reliability of silicon HJT solar modules in which the PLR of PV modules exposed at different locations in the world was collected and reported (Arriaga Arruti et al., 2023). She conducted a statistical analysis on 54 datasets and reported that the median and average PLR is 0.56 and 0.70%/ year respectively. Since, the mean values are sensitive to outliers, the median PLR values of 0.56%/year is considered as an appropriate values for validating the CFM model in MAPLE.

For the validation, 200 locations around the world are chosen randomly from a dataset comprising of the latitude, longitude coordinates, time zone of the city and the country in which is located (GeoNames-Public by Opendatasoft, 2024). The selected locations are shown in Fig. 4. The median predicted PLR of modules from MAPLE is 0.53%/year (see Fig. 6 with a % difference of 5.36% when compared with results reported by Arruti et al. The model parameters of the CFM module for HJT technology is shown in Fig. 5. The model and shape parameters B and μ are 200 and 0.125 respectively. The pre-exponent factors for the degradation processes, A_1 , A_2 and A_3 , are $2e5$, 71.001 and 2.0011 respectively.

The uncertainty propagated by the model due to climatic variations is shown in Fig. 3. Kaaya et al. evaluated the impact of climate variable calculation models, such as the Faiman and Ross models for module temperature, and found that the variability contributed by these models is minimal (Kaaya et al., 2021). Fig. 3 clearly demonstrates that the model is sensitive to ambient temperature, with the highest degradation rate observed in climate As, which denotes a tropical steppe climate. This climate also exhibits the greatest variability due to significant fluctuations in day and night conditions. Such variability directly impacts the thermomechanical degradation rate in the model. Therefore, when assessing performance loss or calculating overall degradation rates at a specific location, it is essential to recognize that degradation rates may vary according to climate classification and should not be generalized.

4.1.2. Caveats of the CFM approach

Although CFM, which is essentially a system-level degradation analysis, is very simple to implement, it has several inherent disadvantages:

- **Degradation modes are unidentifiable:** The modeling strategy cannot resolve different degradation mechanisms triggered by one environmental stressor since it is challenging to incorporate PoFs within the modeling formulation. It can be observed that the activation energies for HJT (see Fig. 5) and mono-Si module show a similar trend i.e. the predominant degradation mechanism is hydrolysis, followed by UV degradation and then temperature cycling. However, we do not obtain information on how the environmental stresses affect the PV technology. For instance, UV might initiate recombination losses (Yang et al., 2024), a degradation mode prevalent in current HJT technologies, along with encapsulant yellowing, while for module with a different technology, it might just initiate yellowing. CFM assumes that the degradation mechanism is similar for a given stressor irrespective of the module technology.



Fig. 2. A typical arrangement of a 60 cell module with 5 substrings inside MAPLE. Cells 1, 12, 51 and 60 are corner cells. Cells 2-12, 13, 25, 26, 38, 39, 50 and 52-59 are side cells.

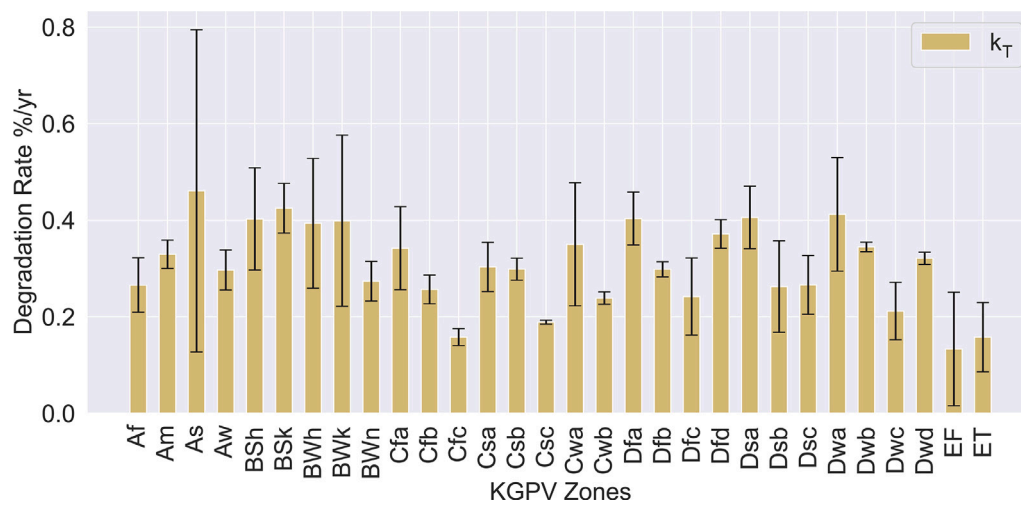


Fig. 3. Degradation rate (%/year) calculated for different climates classified according to the Köppen Geiger climate classification (Rubel et al., 2017). The expansion of the different climate classifications in the figure is given in the supplementary material.

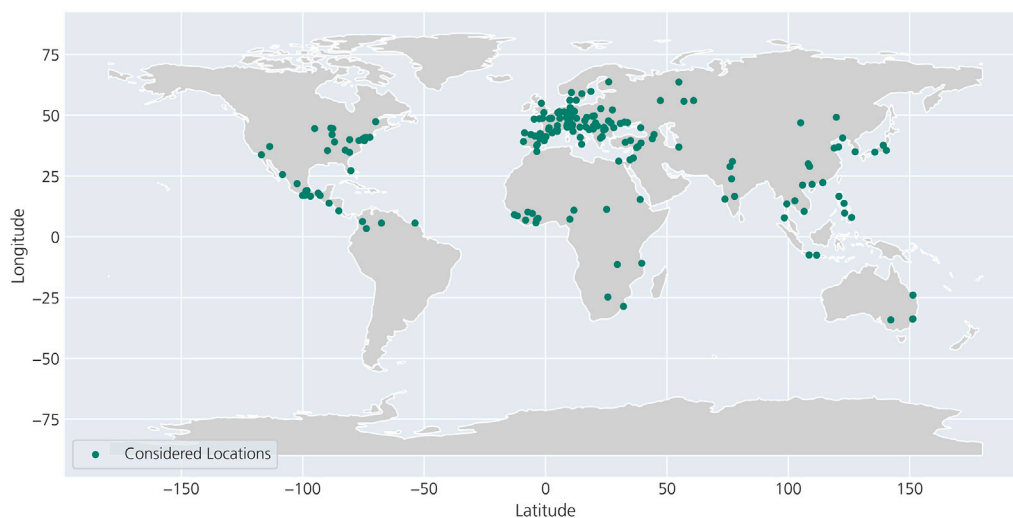


Fig. 4. Selected locations for PLR calculation using CFM strategy.

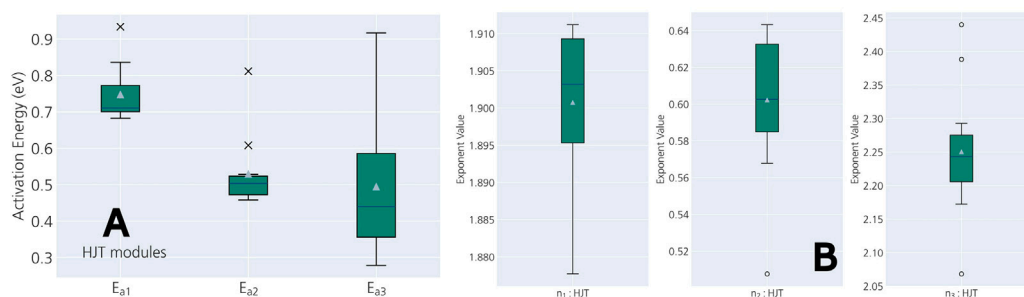


Fig. 5. (A): Activation energies for HJT modules, (B) Model parameters n_1 , n_2 and n_3 .

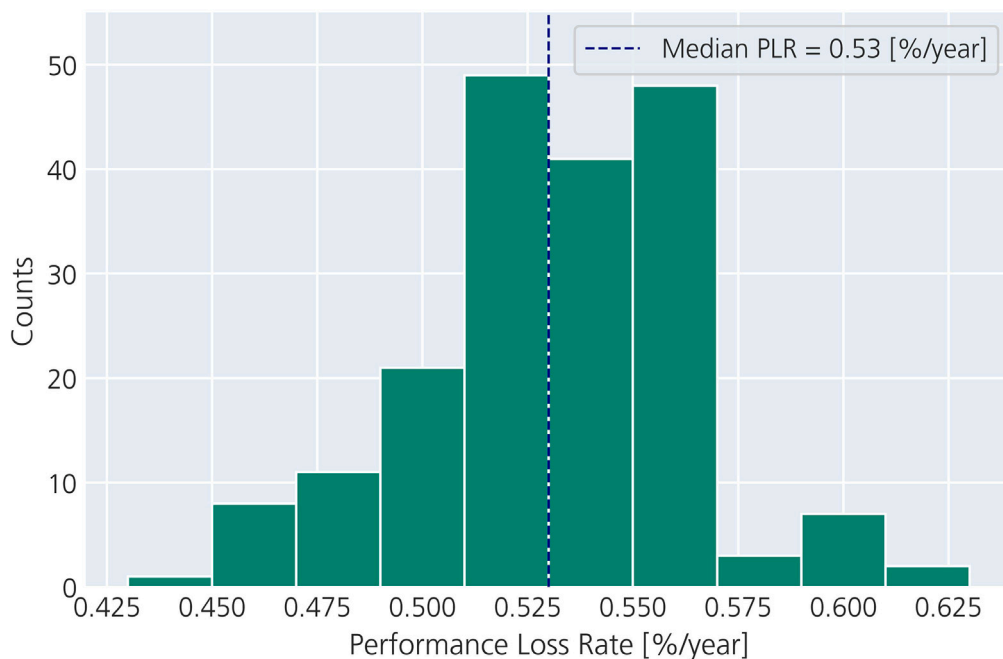


Fig. 6. Histogram of PLR predictions for HJT modules at the considered locations by MAPLE.

- **Combining degradation modes in CFM:** The stresses in CFM are coupled through Eq. (4), which is directly sourced from a report by Gaines et al. (1979b). It is explicitly stated that this formulation cannot accurately represent the effects of individual stresses on overall performance. The choice of this equation is a compromise aimed at minimizing the number of tests while incorporating known behavioral traits, such as the exponential dependence of degradation rate on temperature. This approach allows for the individual degradation rates, k_H, k_{PH}, k_{TC} , to be represented as a product that equals one when any of the rates approaches zero. However, this empirical formulation fails to demonstrate how individual stressors contribute to degradation.
- **Estimates performance loss:** As mentioned in the introduction, system-level degradation models incorporate performance losses from various factors that act as noise. We do not estimate the module degradation explicitly using Eqs. (1), (2) and (3).
- **Calibration through accelerated tests:** CFM strategy uses available field degradation data to fit model parameters. The available field degradation data is from modules with older cell and material technologies. The reported field degradation data could be an artifact, which might not be appropriate to describe the performance of a module with a particular cell technology. With CFM, it is complex to incorporate new degradation data from accelerated tests on modules or module constituents. With cell technology and material research accelerating at a rapid pace, the

quick implementation of CFM to reliably predict degradation in newer technologies is questionable.

- **Modeling regenerative/non-permanent degradation:** CFMs do not accommodate regenerative mechanisms. Fig. 7 illustrates the incapability of CFM strategy to predict the degradation and regeneration in PV performance occurring due to PID, as seen in Fig. 7. Material sensitivities to a degradation mode cannot be modeled and incorporated into the CFM strategy. In this example, the effect of a PID non-sensitive encapsulant is clearly noticeable outdoors. However, CFM simply delivers a power evolution curve at a given location for a module with a prescribed cell technology.

4.2. MSM- a workflow enabling combination and calibration of models

The MSM approach in MAPLE aims to address several significant shortcomings of the CFM approach. A crucial aspect of the MSM approach is its ability to leverage accelerated test data to predict field degradation. To facilitate this, an important concept known as equivalent time is discussed in detail first. Subsequently, we demonstrate how the results of a simple damp-heat test, typically conducted at 85 °C and 85% relative humidity (RH), are extrapolated to field conditions within the MSM module of MAPLE. Finally, we illustrate how the evolution of degradation changes when degradation modes influence each other, as well as when they evolve independently.



Fig. 7. Comparison of CFM's prediction against PID outdoor data from Berghold et al. (2013).

4.2.1. Equivalent time

An important concept when utilizing accelerated test data for field predictions is the concept of equivalent time which has been scarcely discussed in literature (Braisaz et al., 2014; Annigoni, 2018). When iterating over time, the degradation at a given time step should be the cumulative sum of degradation from all previous time steps, along with the degradation occurring in the current time step. The equivalent time approach offers a mathematical framework for achieving this.

In the illustrative explanation (Fig. 8) the green point at t_i shows the jump in power if the environmental stress is lower compared to the value at t_{i-1} . This happens when the time is incremented in an absolute way during iteration. While modeling, it is important to avoid such pseudo regenerative spikes which does not reflect the actual behavior of the degradation process.

To elucidate the working of equivalent time, we consider the example of the DH model in Eq. (10). Here, B is kept as a constant to make the explanation simple.

$$P_{norm} = \frac{1 + \exp(-B)}{1 + \exp(R_d * time - B)} \quad (24)$$

While testing indoors, T is a constant, R_d is a constant and P_{norm} plots a smooth sigmoidal decay curve that starts from 1 and as $t \rightarrow \infty$, becomes zero. However, in outdoor conditions, R_d , given by Eq. (25), varies dynamically. The dynamic component in Eq. (24) is referred to as $K(T)$, as shown in Eq. (26).

$$R_d(T) = A \cdot \exp\left(\frac{-E_a}{k * T}\right) \quad (25)$$

$$K(T) = R_d * time \quad (26)$$

The term $K(T) = R_d * time$ could be written as,

$$K(T) = R_d * i * \Delta t \quad (27)$$

where, $i=1,2,\dots,n$, where n is the last time step, when $\Delta t=1$.

The typical hourly variation of R_d for Singapore, where T does not vary a lot annually, is shown in Fig. 9. In Eq. (27), as $i \rightarrow \infty$, the term

$R_d * i * \Delta t$ gradually grows unstable as shown in Fig. 10. Therefore, when developing an algorithm to compute outdoor degradation, it is important to note that while the indoor model is valid at a specific step, power should not be calculated by simply incrementing the time step using absolute time values. Instead, the time increment for the next step should be determined by cumulatively computing the time required for degradation to reach the current step's values, considering the temperature for the next step and the degradation increment for the chosen step size. This alters the dynamic component of the indoor model (Eq. (24)) as shown in Eq. (28).

$$K_{eq}(T) = R_d * (t_{eq} + \Delta t) \quad (28)$$

The comparison between $K(T)$ and K_{eq} for a period of 25 years is shown in Fig. 10. For a given location, the temperature and relative humidity does not vary largely for a very small time step. Therefore, t_{eq} has less variation when iterating in time, and $t_{eq} + \Delta t$ does not blow up as $i * \Delta t$ did. The use of equivalent time is, therefore, not just intuitive but provides a mathematically valid method for incrementing in time.

4.2.2. Extrapolating indoor damp heat test results to outdoor performance predictions

The MSM workflow has the ability to incorporate degradation data, especially from accelerated tests, of modules with newer materials and cell technologies. This section demonstrates how the MSM module calculates field degradation of a commercial TOPCon module using only indoor damp heat tests conducted under standard conditions. Accelerated tests, based on testing standards (Ex. IEC 61215(IEC, 2021)), are done at constant T and RH at 85 °C and 85% to test for module integrity against corrosion due to moisture ingress.

This example uses Eqs. (10) and (12) to demonstrate the extrapolation of indoor to outdoor results. To determine the parameters of Eq. (12), a multiplication factor is determined from the accelerated test results available in the parent article (Braisaz et al., 2014). The parent article provides the results for R_d and B at two other conditions, at 95 °C/85% RH and 95 °C/58% RH, apart from the standard test condition of 85 °C and 85% RH. From this, the parameters of the

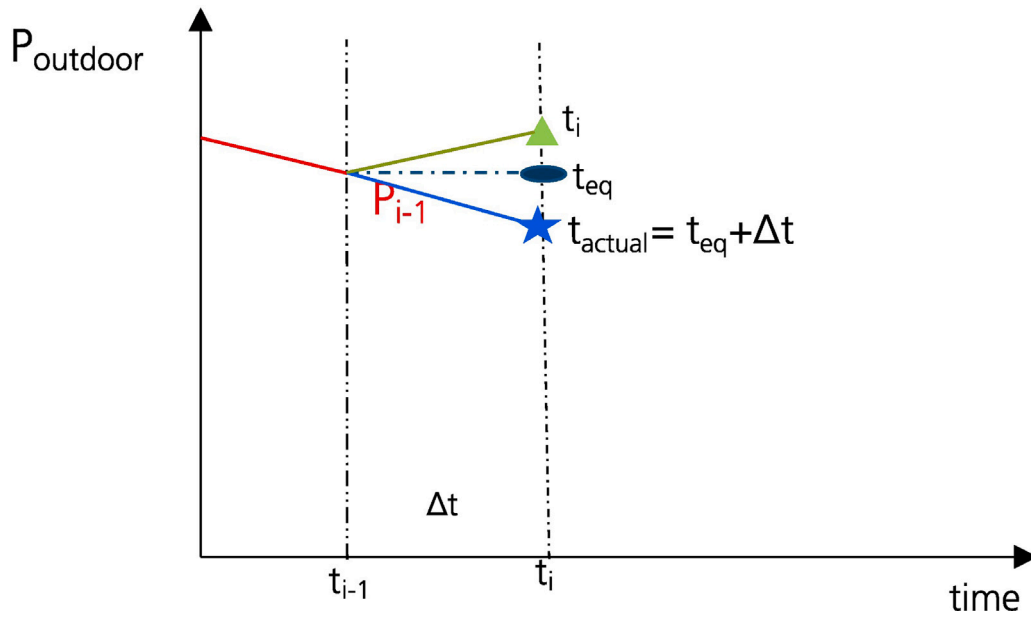


Fig. 8. Power at time increment, t_i (P_i), power calculated at equivalent time, t_{eq} (P_{teq}) and the power computed with the actual time increment during the iteration process ($t_{actual} = t_i + t_{eq}$, P_{actual}). The power at every time step is computed using Eq. (24).

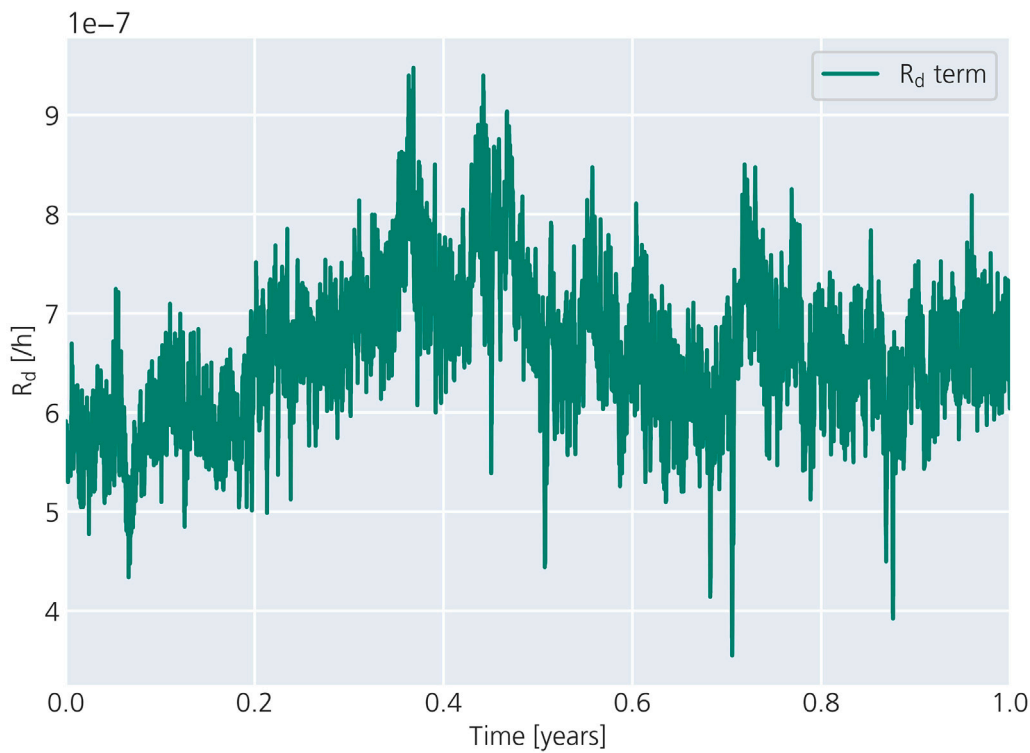


Fig. 9. Degradation rate (R_d) variation according to (28) for Singapore at $\Delta t=1$ h.

Peck’s model (Eq. (12)) are determined. The multiplication factor was determined for the model parameters in Eq. (10) at each of these conditions w.r.t to their parameters at standard conditions i.e. 85 °C and 85% RH is shown below:

$$\frac{R_D^{95\text{ }^\circ\text{C}/85\%}}{R_D^{85\text{ }^\circ\text{C}/85\%}} = 3.1; \quad \frac{R_D^{95\text{ }^\circ\text{C}/58\%}}{R_D^{85\text{ }^\circ\text{C}/85\%}} = 1.5 \quad (29)$$

$$\frac{B^{95\text{ }^\circ\text{C}/85\%}}{B^{85\text{ }^\circ\text{C}/85\%}} = 0.96; \quad \frac{B^{95\text{ }^\circ\text{C}/58\%}}{B^{85\text{ }^\circ\text{C}/85\%}} = 1.01 \quad (30)$$

Eqs. (29) and (30) are used to determine the model parameters, R_d and B , at the other test conditions for the TOPCon modules. The parameters R_d and B for the TOPCon modules at 85 °C and 85%RH are obtained by fitting the indoor test data to Eq. (10), as shown in Fig. 11 Consequently, the parameters in Eq. (12) are determined for the TOPCon modules. Using these values, the field degradation due to the combined effect of T and RH is predicted.

The outdoor degradation path of the TOPCon modules in five different locations with varied climatic conditions is shown in Fig. 12

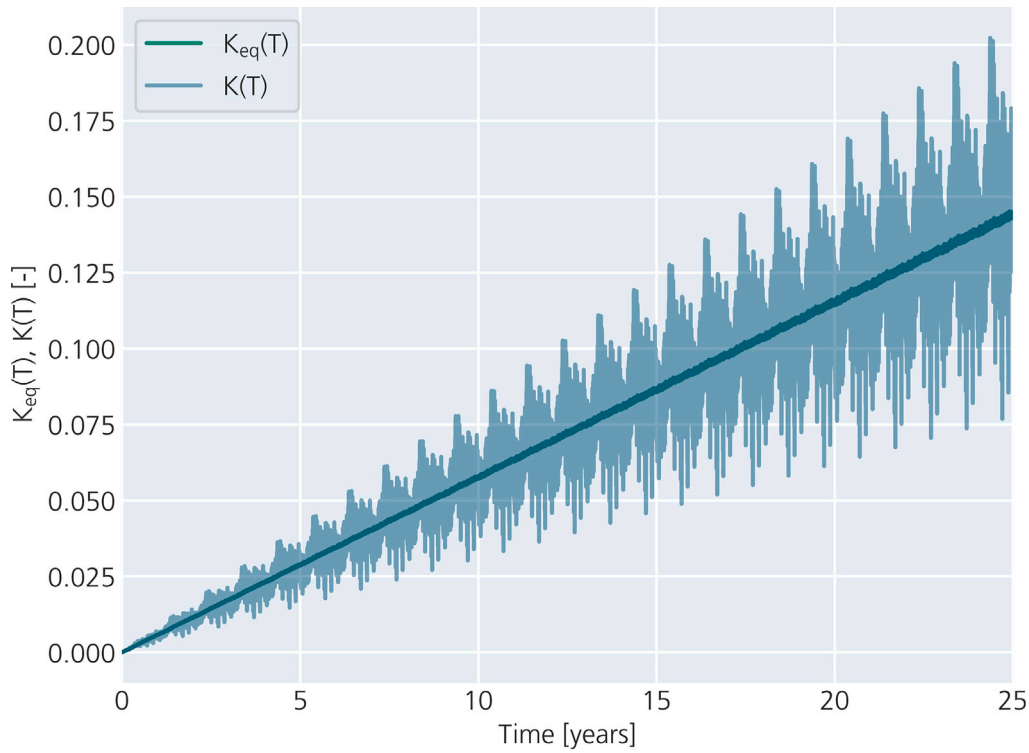


Fig. 10. Comparison of $K(T)$ and $K_{eq}(T)$ for Singapore at $\Delta=1$.

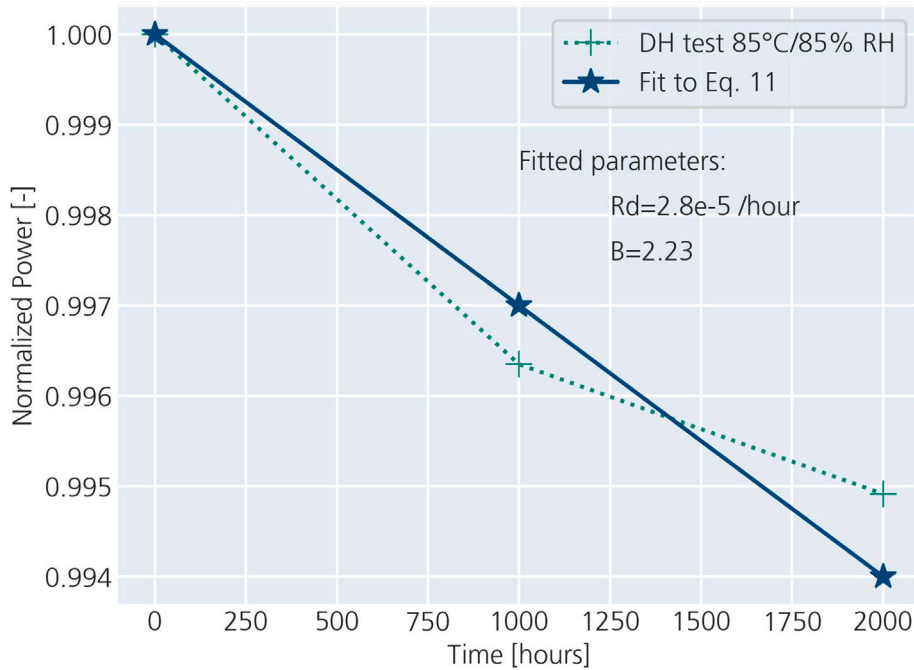


Fig. 11. Indoor DH test data for two TOPCon modules. Data fitted to Eq. (10).

for 20 years. The degradation path depends on the model parameters R_d and B . As R_d increases the slope of the sigmoidal curve while an increase in B pushes the slope more towards the right increasing the induction period (at a given time step). Consequently, R_d and B themselves depend on T_{mod} and RH. From Eq. (30), it is evident that B varies mildly when T and RH is changed when compared to R_d (Eq. (29)).

4.2.3. Combining multiple degradation modes inside MAPLE

Understanding interaction between degradation modes is not trivial and demands expert knowledge on the different degradation modes that might arise in the field. A probability of occurrence of different degradation modes towards the overall degradation in a module installed at a given location is computed by analyzing a large database of field degraded modules (Poddar et al., 2024). The probability of occurrence

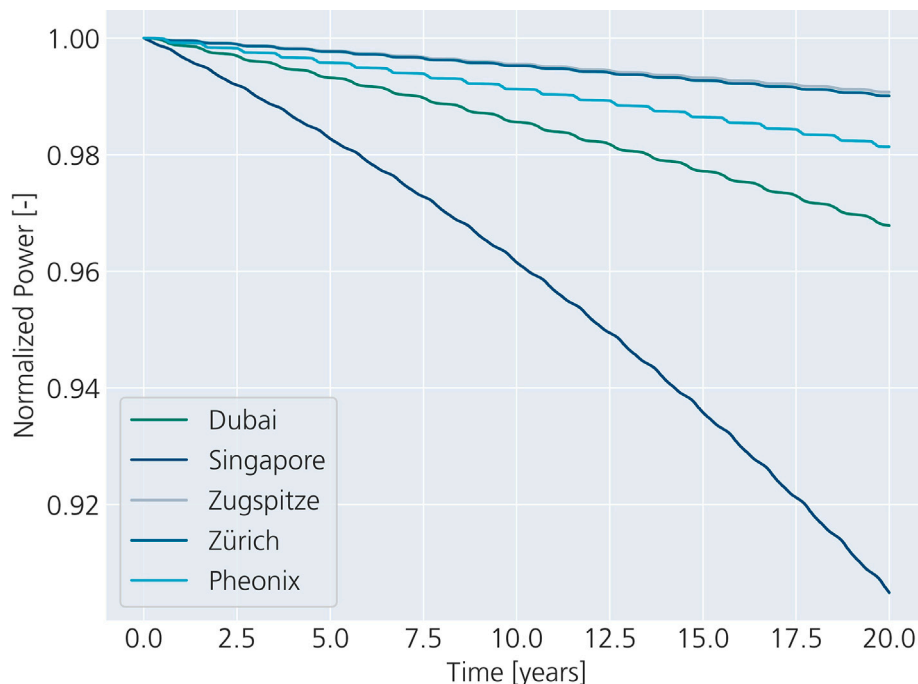


Fig. 12. Predictions of in-field degradation for TOPCon modules due to temperature and humidity stress factors. The model (Braisaz et al., 2014) parameters were adapted using a single DH standard indoor test conducted at 85 °C/85% RH.

is then multiplied to the degradation rates (computed using CFM models) to attenuate or exacerbate a degradation mode. However, the relevance of this approach towards contemporary, and ever evolving, technologies and materials is questionable and hence not adopted here.

MAPLE allows to account for mutually affecting degradation modes as demonstrated for the simultaneous reduction in power due to the increase of series resistance and encapsulation discoloration by Sinha et al. (2016). There, it is reported that the increase in power degradation of the modules due to corrosion induced by the discolored and degraded encapsulant could be as high as 14 %. This effect could be interpreted as a 14 % stronger corrosion effect due to the discoloration of the encapsulants. This approach quantifies the release of acetic acid during encapsulant degradation and discoloration, which induces corrosion of the cell metallization. The combined effect can be accounted for using Eq. (9) by incorporating $k^A=1$, for the discolored degradation measure and $k^B=1.14$ for the corrosion degradation measure. The model parameters determined from the parent article of the degradation model formulations are currently set as default inside MAPLE.

The combined effects of the degradation modes is shown in Fig. 13. In this example, the combination of the DH model (10) along with the discoloration model derived from Miller et al. (Eq. (18)) is compared. The degradation from corrosion due to T and RH (DH) is predicted to be 3.1% from the initial non-degraded state. If encapsulant discoloration is the only degradation mode affecting performance, then the degradation in power amounts to 12.5% (black solid line). When the modes, corrosion and discoloration, happen simultaneously and are independent, the degradation amounts to 15.2%. The dependent effects are shown when corrosion is exacerbated by discoloration of encapsulants (red dashed line), increasing the degradation to 15.6%. The importance of determining the dominant failure modes is shown to be critical here in this example where the increase in corrosive degradation due to encapsulant discoloration affects the total power output of the module. It should be noted that using this feature of MAPLE requires a detailed understanding of the physics behind the initiation and progression of a degradation mode.

Additional examples on the implementation of the MSM method is shown in Figs. 14 and 15. The Fig. 14 shows the cyclic effect of the PID model which occurs due to the seasonal effect. A closer look on the seasonality effect on the power evolution is shown in the inset of the figure. The rainy season spans from mid-April to September in Miami. This period clearly shows a degradation trend, after which the trend inverts slowly (mid-September to April) due to the dry season in Miami (Annigoni, 2018). The change point model as described by Ren et al. is extrapolated to outdoor conditions for a desert and polar climatic condition to showcase the effect of UV dose on modules with UV pass and UV cut encapsulants, as shown in Fig. 15.

MSM's ability to combine degradation modes is well-suited for calculating the degradation kinetics of bifacial PV modules. Recent LCOE analyses indicate that bifacial modules are more cost-effective than their monofacial counterparts, particularly in temperate and polar climates (Rodríguez-Gallegos et al., 2018). Bifacial modules face several degradation mechanisms, including PID-s (shunting type), PID-p (polarization type), UV-induced degradation from UV-transmitting encapsulants, and LeTID, among others (Bartholomäus et al., 2025; Stein et al., 2021). Ovaitt et al. compared the degradation of critical IV parameters between different bifacial cell technologies and their monofacial counterparts, concluding that the back surface degrades faster than the front for all IV parameters (Ovaitt et al., 2024). These findings are crucial as they separately address degradation on the front and back surfaces of the cell. However, the currently available models only consider the degradation on the front side. When special considerations for bifaciality become available in the community, they can be easily incorporated into MAPLE, owing to its modularity.

4.3. Caveats of the MSM approach

MSM addresses some shortcomings of the CFM approach, particularly the ability to add new models and calibrate existing ones to reflect the degradation kinetics of newer materials. However, the MSM approach has its own limitations, which are described below:

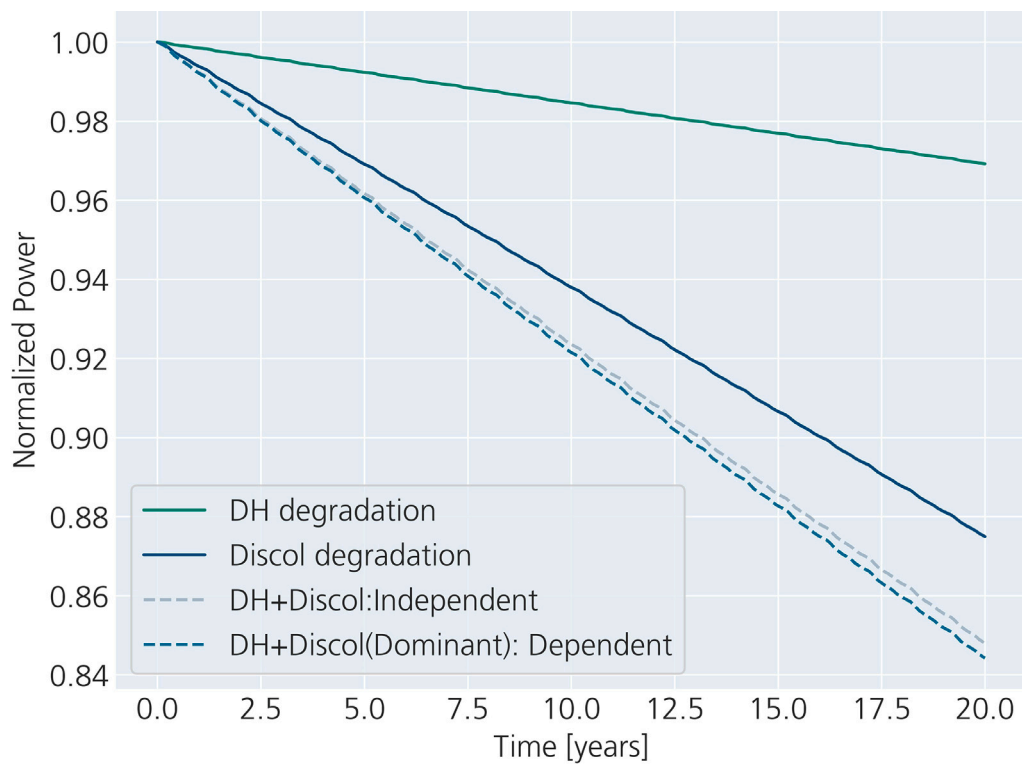


Fig. 13. Combined degradation effect of discoloration and corrosion in PV modules.

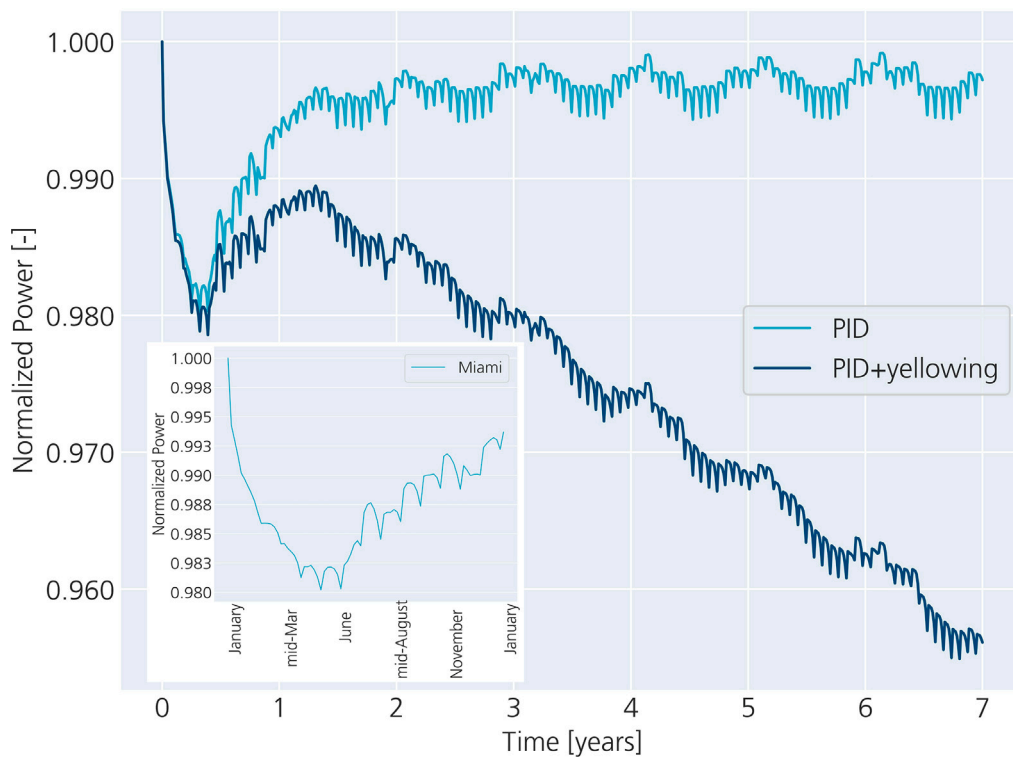


Fig. 14. PID-s effect modeled as described by Annigoni et al. in Section 3.2.4 of this article for Miami. Discoloration is modeled as an independent event.

• **A Non-Plug-and-Play Solution:** The models used in this approach are available in literature and were developed for PV module types in the past. As stated earlier, it is very possible that another combination of materials, module design, cell type etc. might cause a different degradation evolution and negate

claims such as the dependence between discoloration and corrosion modes. This highlights the importance of understanding the interaction between degradation modes and constant calibration of the models inside MAPLE when new degradation data is available. Unfortunately, quantifying interaction between modes

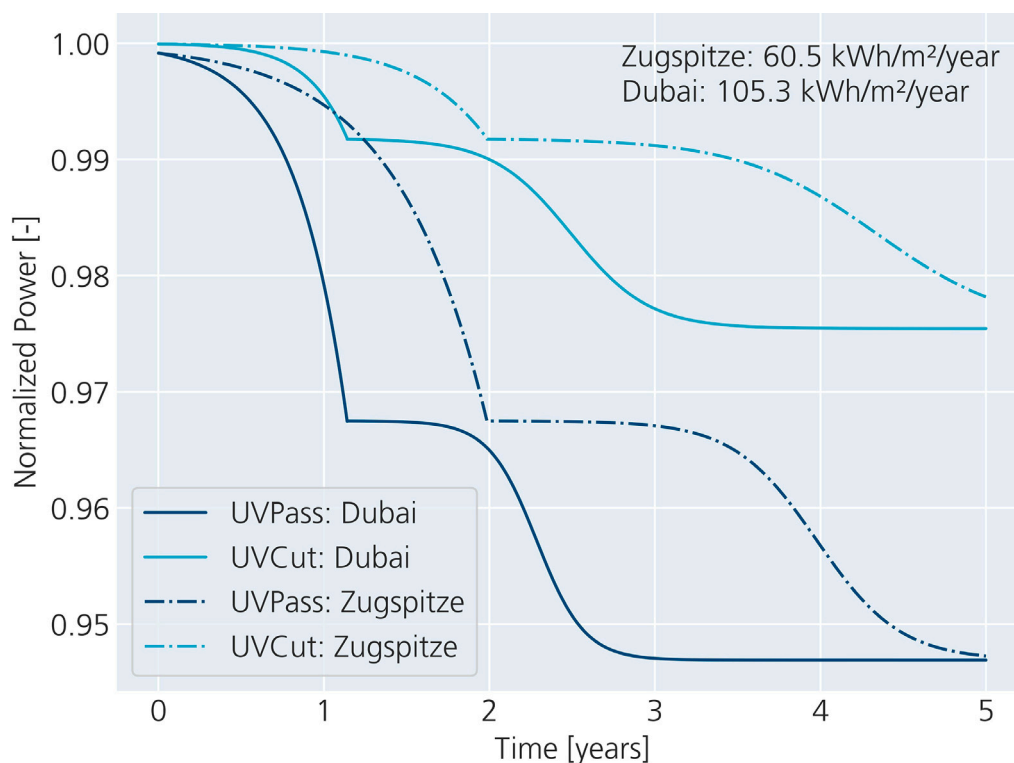


Fig. 15. UV induced degradation in HJT modules modeled using the change point regression model as prescribed by Ren et al. (2024) in Section 3.2.2 of this article.

is a challenging task due to the ever-changing material landscape within the PV industry and also the resources that would be needed to conduct such a study.

- **Artifact Degradation:** Models are usually developed based on a specific degrading module type or material. It is unclear how well this example represents other PV modules from the same production period, technology, or materials. For instance, the degradation illustrated in Fig. 13 appears significant when paired with a discoloration model, but the degree of discoloration may not apply to all modules. This issue is often overlooked in literature on degradation model development.
- **Homogenized Degradation:** Although MSM approaches are quite flexible to predict and combine different degradation modes and their effect on the power output of the whole module, the approach considers the degradation to be homogenized across the whole module. Predominantly, degradation modes affect different parts of the cells differently as seen in the case of encapsulant discoloration (Sinha et al., 2016), delamination (Meena et al., 2024), finger degradation due to thermomechanical fatigue (Kumar and Gupta, 2018), PID (Tong et al., 2024) etc. This requires a different modeling strategy where the degradation mode's influence on cell level is aggregated to compute module level performance.
- **Unavailability of models:** Another glaring disadvantage is the unavailability of models or their parameters in literature to describe several degradation modes, especially for newer materials and module technologies. For example, modeling the degradation of multilayer EPE encapsulants might prove a challenge only by using models from Sinha et al. or Miller et al. data. In the future, MAPLE's MSM library will be updated constantly using collected and formulated models and material properties.
- **Uncertainty quantification:** Uncertainty in modeling results stems from input climatic data, material degradation data, and model assumptions (Kaaya et al., 2021). In the MSM approach, we utilize parametric models primarily calibrated using indoor test results, which are then extrapolated outdoors using the equivalent

time approach. Many of the studies reported calibrate activation energies and other model parameters empirically, often relying on just one or two experimental samples. Consequently, numerous studies lack concrete data on uncertainties in degradation parameters due to material and degradation kinetics. Furthermore, the uncertainty statistics related to climatic data will vary depending on the source utilized. The authors wish to highlight that such analyses can be effectively performed within MAPLE by calculating degradation rates and parameters while linking the degradation models to diverse climate data retrieved from various sources.

4.4. MFM- a bottom-up approach towards degradation modeling

Cells inside a PV module do not always degrade similarly due to localized stressors (e.g. moisture gradients (Mittag et al., 2017a), hail damage) or localized sensitivities (e.g. LeTID (Johnston et al., 2021) or UVID). This is accounted for by the multi-scale failure modeling (MFM) strategy which aggregates electrical properties of cells inside a module. Firstly, we present an illustration of moisture driven corrosion in PV modules to demonstrate the motivation towards the perspective of modeling degradation using a bottom-up approach. After this we present a verification for the working of the MFM module using a module that is damaged inhomogeneously.

4.4.1. Motivation for the development of MFM approach

Degradation models that support a bottom-up approach is scarce in literature. Unlike models in MSM which tracks degradation as a function of time, degradation models supporting MFM should measure the degradation of a solar cell as a function of space and time inside the module. Let us consider moisture-driven corrosion inside a glass module, illustrated in Fig. 16 (Ravindrababu et al., 2023).

After sufficient moisture ingress, the degradation process render cells which have different states: Cells near the edges may be completely degraded, with degradation effects diminishing towards the

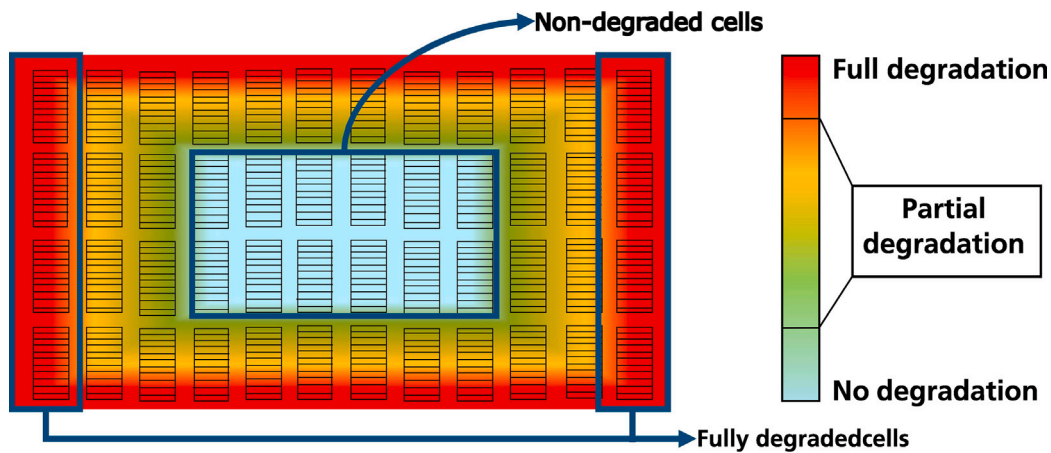


Fig. 16. Different stages of cell degradation in a module which warrants the MFM approach.

center. To gauge the performance of the partially degraded cells, a more accurate approach would be to account for varying water concentration at different locations inside the module. This approach requires a surrogate model that computes the moisture concentration, locally within the module, as a function of ambient temperature and relative humidity, e.g. an empirical model based on FEM modeling. This moisture concentration is then used by MAPLE to compute the degradation in the cell properties and subsequently the degradation of the whole module. This lack of integration is currently not implemented primarily due to the absence of validated degradation model formulations in the literature to compute the overall performance degradation of the module. One could argue that DH induced degradation could be modeled with standard DH tests as illustrated in the MSM section of this paper. However, a first principle approach, such as MFM, might yield more accurate results in the longer run when more experiments towards characterizing cell performance against moisture concentration get reported. One big advantage are the reduction in testing costs since the testing might involve only mini-modules and the accuracy of degradation prediction will be several folds higher than the MSM approach. Furthermore, PoFs can be used to describe the degradation of PV materials probabilistically, as reported by Pintar et al. (2020). A probabilistic description of the service lifetime is possible if the modeling framework is able to simulate degradation at different length scales (Hartley, 2019).

A bottom-up approach also facilitates the integration of losses with degradation occurring during field operations. For example, the effects of shading, temperature, and irradiance differences due to soiling or snow on module power can be studied by combining the MFM degradation module with tools for analyzing loss channels in PV modules, such as SmartCalc.Module, a cell-to-module loss tool from Fraunhofer ISE (Mittag et al., 2017b). This integration ensures a holistic approach towards the accurate prediction of magnitude of degradation, bringing the community closer to accurately predicting the module service lifetime.

4.4.2. Verification of MFM implementation using hail impacted modules

As an example to showcase this functionality in MAPLE, we simulate the loss in power due to non-uniformly developed cell cracks during an indoor hail impact test.

Module subjected to indoor hail tests and the electroluminescence (EL) image is shown in Fig. 17. Cells with cracks in a PV module can be classified into four types: A, B, B+C and C cracks (Spataru et al., 2017). The appearance of these cracks in a module during an outdoor hail event is random and is affected by the module properties, hail characteristics (size and severity of hailstones, windspeed etc.), and the boundary conditions (mounting, frame type etc.) of the modules (Mathiak et al., 2016). The crack classification is done by

comparing EL images of the PV module taken at different current bias settings and calculating the low EL intensity (LEL) as exhibited by Spataru et al. (2017). A and C cracks can be easily identified visually from the EL images. A cracks refer to mildly cracked regions where the active parts of the cell remain intact, resulting in minimal power loss. EL intensities do not change according to the bias current while characterizing an A crack. In contrast, C cracks are the most malignant, indicating cells that are completely disconnected from active cell area, consequently reducing the power. The area of cells with C crack appear dark irrespective of the current bias setting.

In the case of B and B+C cracks, EL images might show different behavior depending on the how the crack has developed in the cell. In this work, we denote cracks as cells that show a low EL intensity in low-bias current settings with the letter B, while cracks show darker areas in high bias current EL image while becoming darker in the low bias current setting as B+C. The difference in the EL intensities in images results from the partial damage induced by mechanical impact and the specific type of damage (B or B+C) caused by the crack in the cell (IEC, 2018). Apart from increase in series resistance in the cell due to the partial disconnection, cracks might also induce shunts in the cell (Kumar and Gupta, 2024). The IEC 60904-13 standard on EL of PV modules states that a shunted cell might appear dark in a low current bias EL image, while a cell affected by series resistance will show lower contrast at low current bias due to reduced voltage losses across the cracks.

For simulating the power loss in a hail impacted module, the individual loss in cell performance parameters due to A, B, B+C and C cracks were established based on tests on small-scale modules by Spataru et al. (2015). Since A cracks are the most benign, the cell which suffered the smallest loss in I_{sc} , R_s and R_{sh} was considered to calculate the scaling factor for A cracks in Table 2. Similarly, for C cracks, the cell with the strongest performance loss was considered. To classify between cells which suffered only B and B+C cracks, the calculated values from Santamaria et al. containing the LEL of B and C cracks of the cells was taken as the reference. We assumed that cells which have less than 5 % LEL for C cracks are affected only by B cracks, so the average degradation was used as a reference for cells of type B and B+C. The percentage reduction in the IV properties are expressed as a loss factor. In the same way, cells which had more than 5 % LEL were considered to be affected by both B and C cracks, the average percentage reduction of such cells were used to calculate a scaling factor for cells affected by B+C cracks. The scaling factors used in the calculation inside MAPLE is shown in Table 2.

The performance of MAPLE to predict the relative loss in maximum power is shown in Table 3. The correlation of IV characteristics of a cracked cell based on the composition of B and C cracks by calculating the LEL, as shown in Santamaria et al. could be erroneous since we

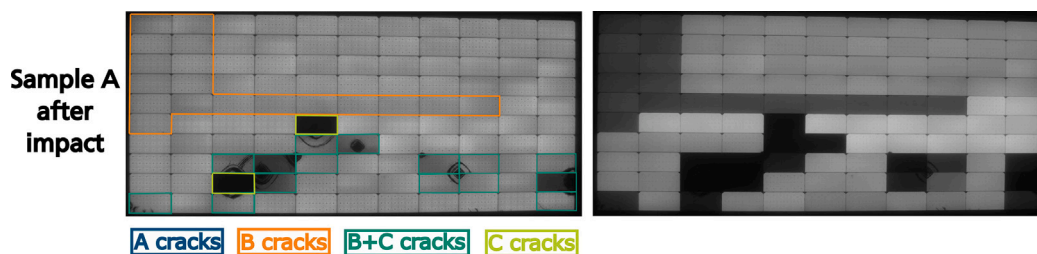


Fig. 17. Initial and after impact EL image of module at I_{sc} and 10% I_{sc} bias.

Table 2

Loss factors for I_{sc} , R_s and R_{sh} for the different cracks.

Parameters	A cracks	B cracks	B+C cracks	C cracks
I_{sc}	0.97	0.975	0.876	0.845
R_s	1.1	1.324	1.692	2.62
R_{sh}	0.852	0.896	0.568	0.632

Table 3

Comparison of relative to initial P_{mpp} experimental versus simulation results of Sample A.

	Experiment	Simulation	% Deviation
Sample A	-8%	-7.54%	5.75%

find that similar percentages of B and C cracks in a cell could result in completely different IV loss characteristics. The percentage deviation of the simulated results is 5.75%, which could be further improved by correlating properties to cracked cells through a data-driven approach, as demonstrated by Turek et al. who uses an artificial neural network to classify damages in a cell (Turek and Meusel, 2023). Nevertheless, such methodologies could be integrated into MFM to study locally induced damages in a module.

5. Conclusions and future work

This paper presents the development of a comprehensive degradation modeling framework, termed MAPLE, which functions as a modular tool for calculating degradation in photovoltaic (PV) modules under field conditions through established degradation modeling strategies. The models and approaches outlined herein are applicable to modules featuring any cell architecture (c-Si, perovskites, Si-tandem etc.), contingent upon the availability of the requisite inputs. We have integrated existing models from the literature, enhancing the CFM modeling strategy by identifying activation energies and new model parameters for emerging cell technologies, particularly heterojunction modules. The MSM strategy incorporates analytical models specifically designed to investigate degradation modes and has been adapted to employ accelerated test data for newer technologies, such as TOPCon modules. Furthermore, the MSM strategy includes a straightforward multiplicative degradation modeling equation that aggregates degradation from various modes. We elucidate the concept of equivalent time, which computes cumulative degradation iteratively over time, applied to several indoor-derived rate models for outdoor degradation assessment. Additionally, an introductory example demonstrating the capabilities of the MFM strategy is provided, highlighting the aggregation of diverse cell properties resulting from the varying distribution of hail impact damage. We assert that MFM possesses significant potential for accurately computing degradation due to its foundation in first principles. The exploration of characterizing each degradation mode using first principles represents a valuable direction for future research.

It is crucial to emphasize that MAPLE is an evolving framework that presents a variety of methodologies for modeling degradation in photovoltaic (PV) modules. By streamlining the implementation of

these strategies, MAPLE significantly enhances the models' accessibility for the PV community. Its evolution is anticipated as newer models and algorithms become available.

Future research will focus on refining models that combine degradation modes within the MSM framework. The multiplicative model presented here computes total degradation by normalizing output power across individual degradation modes; however, the interactions among different modes remain complex and warrant further exploration. A comprehensive understanding of these interactions can only be achieved through extensive experimental studies where a combination of stressors act simultaneously. Moreover, degradation models employing a multi-scale approach, i.e. considering degradation on both cell-and module level, are currently lacking in the literature, and their integration into the framework may necessitate additional algorithmic adjustments, which will be examined in future work.

CRedit authorship contribution statement

Suraj Ravindrababu: Writing – original draft, Visualization, Software, Formal analysis, Data curation, Conceptualization. **Ingrid Hädrich:** Writing – review & editing, Supervision, Funding acquisition. **Ulrich W. Paetzold:** Writing – review & editing, Supervision. **Paul Gebhardt:** Writing – review & editing, Supervision, Funding acquisition, Conceptualization.

Code availability

The MAPLE code is available at: <https://gitlab.cc-asp.fraunhofer.de/maple/maple>. Please contact the corresponding author for further questions.

Declaration of generative AI in scientific writing

The authors declare that generative AI has only been used in the writing process to check for grammatical errors and improve the readability of the text.

Declaration of competing interest

The authors declare that they have no known competing financial interests or personal relationships that could have appeared to influence the work reported in this paper.

Acknowledgments

Funding was provided by the Federal Ministry for Economic Affairs and Energy (FKz.: 03EE1149 A “MiMoRisk”)

Appendix A. Supplementary data

Supplementary material related to this article can be found online at <https://doi.org/10.1016/j.egy.2026.109323>.

Data availability

The MAPLE code is available at: <https://gitlab.cc-asp.fraunhofer.de/maple/maple>. Please contact the corresponding author for further questions.

References

- Aghaei, M., Fairbrother, A., Gok, A., Ahmad, S., Kazim, S., Lobato, K., Oreski, G., Reinders, A., Schmitz, J., Theelen, M., Yilmaz, P., Kettle, J., 2022. Review of degradation and failure phenomena in photovoltaic modules. *Renew. Sustain. Energy Rev.* 159, 112160. <http://dx.doi.org/10.1016/j.rser.2022.112160>, URL <https://www.sciencedirect.com/science/article/pii/S1364032122000880>.
- Annigoni, E., 2018. Reliability of photovoltaic modules: from indoor testing to long-term performance prediction. Tech. rep., EPFL.
- Arriaga Arruti, O., Virtuani, A., Ballif, C., 2023. Long-term performance and reliability of silicon heterojunction solar modules. *Prog. Photovolt., Res. Appl.* 31 (7), 664–677. <http://dx.doi.org/10.1002/pip.3688>, URL [arXiv:https://onlinelibrary.wiley.com/doi/pdf/10.1002/pip.3688](https://onlinelibrary.wiley.com/doi/pdf/10.1002/pip.3688).
- Aydin, O., Yassikaya, M.Y., 2022. Validity and reliability analysis of the PlotDigitizer software program for data extraction from single-case graphs. *Perspect. Behav. Sci.* 45 (1), 239–257.
- Bartholomäus, M., Riedel-Lyngskær, N., Morino, L., Dhimish, M., Stefanidis, P., Razzanako, I., Deru, M., Poulsen, P.B., Spataru, S.V., 2025. Field degradation of bifacial photovoltaic modules in northern Europe. *Sol. Energy* 300, 113786.
- Berghold, J., Grunow, P., Hacke, P., Herrmann, W., Hoffmann, S., Janke, S., Jaekel, B., Koch, S., Koehl, M., Mathiak, G., et al., 2013. PID test round robins and outdoor correlation. In: *Proc. of the 28th European Photovoltaic Solar Energy Conference*, vol. 3003, p. 2013.
- Bosco, N., Silverman, T.J., 2021. Solder bond fatigue is insensitive to module size. *IEEE J. Photovolt.* 11 (4), 1048–1050. <http://dx.doi.org/10.1109/JPHOTOV.2021.3074056>.
- Braisaz, B., Duchayne, C., Van Iseghem, M., Radouane, K., 2014. PV aging model applied to several meteorological conditions. In: *Proceedings of the 29th European Photovoltaic Solar Energy Conference and Exhibition (EUPVSEC)*, Amsterdam, the Netherlands. pp. 22–26.
- Carigiet, F., Brabec, C.J., Baumgartner, F.P., 2021. Long-term power degradation analysis of crystalline silicon PV modules using indoor and outdoor measurement techniques. *Renew. Sustain. Energy Rev.* 144, 111005.
- Charki, A., Laronde, R., Bigaud, D., 2013. Accelerated degradation testing of a photovoltaic module. *J. Photonics Energy* 3 (1), 033099. <http://dx.doi.org/10.1117/1.JPE.3.033099>.
- Chiacchio, F., Aizpurua, J.I., Compagno, L., Moheb Khodayee, S., D'Urso, D., 2019. Modelling and resolution of dynamic reliability problems by the coupling of simulink and the stochastic hybrid fault tree object oriented (SHYFTOO) library. *Information* 10 (9), 283.
- De Soto, W., Klein, S.A., Beckman, W.A., 2006. Improvement and validation of a model for photovoltaic array performance. *Sol. Energy* 80 (1), 78–88.
- Deceglie, M.G., Jordan, D., Nag, A., Deline, C.A., Shinn, A., 2018. RdTools: An open source python library for PV degradation analysis. Tech. rep., National Renewable Energy Lab.(NREL), Golden, CO (United States).
- Eitner, U., Köntges, M., Brendel, R., 2009. Measuring thermomechanical displacements of solar cells in laminates using digital image correlation. In: *2009 34th IEEE Photovoltaic Specialists Conference*. PVSC, pp. 001280–001284. <http://dx.doi.org/10.1109/PVSC.2009.5411248>.
- Escobar, L.A., Meeker, W.Q., 2006. A review of accelerated test models. *Statist. Sci.* 552–577.
- Faiman, D., 2008. Assessing the outdoor operating temperature of photovoltaic modules. *Prog. Photovolt., Res. Appl.* 16 (4), 307–315.
- Fairbrother, A., Gnocchi, L., Ballif, C., Virtuani, A., 2022. Corrosion testing of solar cells: Wear-out degradation behavior. *Sol. Energy Mater. Sol. Cells* 248, 111974. <http://dx.doi.org/10.1016/j.solmat.2022.111974>, URL <https://www.sciencedirect.com/science/article/pii/S0927024822003920>.
- Fokuhl, E., Philipp, D., Mühlhöfer, G., Gebhardt, P., 2021. LID and LETID evolution of PV modules during outdoor operation and indoor tests. *EPJ Photovolt.* 12, 9.
- Gaines, G., Thomas, R., Derringer, G., Kistler, C., Bigg, D., Carmichael, D., 1977. Methodology for designing accelerated aging tests for predicting life of photovoltaic arrays. Tech. rep., U.S. Energy Research and Development Administration, Division of Solar Energy.
- Gaines, G., Thomas, R., Noel, G., Shilliday, T., Wood, V., Carmichael, D., 1979a. Development of an accelerated test design for predicting the service life of the solar array at Mead, Nebraska. Tech. rep., U.S. Energy Research and Development Administration, Division of Solar Energy.
- Gaines, G., Thomas, R., Noel, G., Shilliday, T., Wood, V., Carmichael, D., 1979b. Development of an accelerated test design for predicting the service life of the solar array at Mead, Nebraska. Tech. rep., U.S. Energy Research and Development Administration, Division of Solar Energy.
- GeoNames-Public by Opendatasoft, 2024. Geonames-all-cities-with-a-population-1000@public. Dataset. URL <https://data.opendatasoft.com/pages/home/>.
- Gnocchi, L., Arruti, O.A., Ballif, C., Virtuani, A., 2024. A comprehensive physical model for the sensitivity of silicon heterojunction photovoltaic modules to water ingress. *Cell Rep. Phys. Sci.* 5 (1).
- Gupta, V., Sharma, M., Pachauri, R., Babu, K.D., 2022. Impact of hailstorm on the performance of PV module: a review. *Energy Sources, Part A: Recover. Util. Environ. Eff.* 44 (1), 1923–1944.
- Hacke, P., Spataru, S., Terwilliger, K., Perrin, G., Glick, S., Kurtz, S., Wohlgenuth, J., 2015. Accelerated testing and modeling of potential-induced degradation as a function of temperature and relative humidity. *IEEE J. Photovolt.* 5 (6), 1549–1553. <http://dx.doi.org/10.1109/JPHOTOV.2015.2466463>.
- Hacke, P., Terwilliger, K., Glick, S., Trudell, D., Bosco, N., Johnston, S., Kurtz, S., 2010. Test-to-failure of crystalline silicon modules. In: *2010 35th IEEE Photovoltaic Specialists Conference*. pp. 000244–000250. <http://dx.doi.org/10.1109/PVSC.2010.5614472>.
- Hamed, T.A., Adamovic, N., Aeberhard, U., Alonso-Alvarez, D., Amin-Akhlighi, Z., Der Maur, M.A., Beattie, N., Bednar, N., Berland, K., Birner, S., et al., 2018. Multiscale in modelling and validation for solar photovoltaics. *EPJ Photovolt.* 9, 10.
- Hartley, J.Y., 2019. Multi-scale multi-physics modeling for PV Reliability. Tech. rep., Sandia National Lab.(SNL-NM), Albuquerque, NM (United States).
- Hartley, J., 2021. An integrated, multi-physics, multi-scale modeling capability for pv stressors and failures.. Sandia National Lab.(SNL-NM), Albuquerque, NM (United States).
- Holmgren, W.F., Hansen, C.W., Mikofski, M.A., 2018. Pvlpy python: A python package for modeling solar energy systems. *J. Open Source Softw.* 3 (29), 884.
- IEC, 2018. Photovoltaic devices - Part 13: Electroluminescence of photovoltaic modules. IEC, Geneva, CH.
- IEC, 2021. Photovoltaic (PV) Modules for Terrestrial Applications—Construction Qualification and Type Approval—Part 2: Test Methods, vol. 2000, IEC, Geneva, CH.
- Ishii, T., Choi, S., Sato, R., Chiba, Y., Masuda, A., 2018. Annual degradation rates of recent c-si PV modules under subtropical coastal climate conditions. In: *2018 IEEE 7th World Conference on Photovoltaic Energy Conversion (WCPEC)(a Joint Conference of 45th IEEE PVSC, 28th PVSEC & 34th EU PVSEC)*. IEEE, pp. 705–708.
- Jain, A., Kapoor, A., 2004. Exact analytical solutions of the parameters of real solar cells using Lambert W-function. *Sol. Energy Mater.* 81 (2), 269–277.
- Jang, J.-H., Hong, S.-B., Kim, J.-G., Goo, N.-S., Yu, W.-R., 2021. Accelerated testing method for predicting long-term properties of carbon fiber-reinforced shape memory polymer composites in a low earth orbit environment. *Polymers* 13 (10), 1628.
- Jensen, A.R., Anderson, K.S., Holmgren, W.F., Mikofski, M.A., Hansen, C.W., Boeman, L.J., Loonen, R., 2023a. Pvlpy iotools—Open-source python functions for seamless access to solar irradiance data. *Sol. Energy* 266, 112092.
- Jensen, A.R., Anderson, K.S., Holmgren, W.F., Mikofski, M.A., Hansen, C.W., Boeman, L.J., Loonen, R., 2023b. Pvlpy iotools—Open-source python functions for seamless access to solar irradiance data. *Sol. Energy* 266, 112092. <http://dx.doi.org/10.1016/j.solener.2023.112092>, URL <https://www.sciencedirect.com/science/article/pii/S0038092X23007260>.
- Johnston, S., Xiao, C., Deceglie, M.G., Gaulding, A., Jiang, C.-S., Guthrey, H., Kern, D.B., Kroeger, G.F., Al-Jassim, M., Repins, I.L., 2021. Letid-affected cells from a utility-scale photovoltaic system characterized by deep level transient spectroscopy. In: *2021 IEEE 48th Photovoltaic Specialists Conference. PVSC, IEEE*, pp. 2276–2278.
- Jordan, D.C., Deceglie, M.G., Kurtz, S.R., 2016. PV degradation methodology comparison—A basis for a standard. In: *2016 IEEE 43rd Photovoltaic Specialists Conference. PVSC, IEEE*, pp. 0273–0278.
- Jordan, D.C., Deline, C., Johnston, S., Rummel, S.R., Sekulic, B., Hacke, P., Kurtz, S.R., Davis, K.O., Schneller, E.J., Sun, X., et al., 2017a. Silicon heterojunction system field performance. *IEEE J. Photovolt.* 8 (1), 177–182.
- Jordan, D.C., Deline, C., Kurtz, S.R., Kimball, G.M., Anderson, M., 2017b. Robust PV degradation methodology and application. *IEEE J. Photovolt.* 8 (2), 525–531.
- Jordan, D.C., Deline, C., Kurtz, S.R., Kimball, G.M., Anderson, M., 2017c. Robust PV degradation methodology and application. *IEEE J. Photovolt.* 8 (2), 525–531.
- Jordan, D.C., Haegel, N., Barnes, T.M., 2022. Photovoltaics module reliability for the terawatt age. *Prog. Energy* 4 (2), 022002.
- Kaaya, I., Ascencio-Vásquez, J., Weiss, K.-A., Topić, M., 2021. Assessment of uncertainties and variations in PV modules degradation rates and lifetime predictions using physical models. *Sol. Energy* 218, 354–367.
- Kaaya, I., Chowdhury, G., Morlier, A., 2023. A physics based approach for PV lifetime and degradation signatures prediction. In: *2023 IEEE 50th Photovoltaic Specialists Conference. PVSC, IEEE*, pp. 1–3.
- Kaaya, I., Koehl, M., Mehili, A.P., de Cardona Mariano, S., Weiss, K.A., 2019. Modeling outdoor service lifetime prediction of PV modules: effects of combined climatic stressors on PV module power degradation. *IEEE J. Photovolt.* 9 (4), 1105–1112.
- Kaaya, I., Lindig, S., Weiss, K.-A., Virtuani, A., Sidrach de Cardona, M., Moser, D., 2020. Photovoltaic lifetime forecast model based on degradation patterns. *Prog. Photovolt., Res. Appl.* 28 (10), 979–992. <http://dx.doi.org/10.1002/pip.3280>, URL [arXiv:https://onlinelibrary.wiley.com/doi/pdf/10.1002/pip.3280](https://onlinelibrary.wiley.com/doi/pdf/10.1002/pip.3280).

- Koehl, M., Heck, M., Wiesmeier, S., 2012. Modelling of conditions for accelerated lifetime testing of humidity impact on PV-modules based on monitoring of climatic data. *Sol. Energy Mater. Sol. Cells* 99, 282–291.
- Kumar, S., Gupta, R., 2018. Investigation and analysis of thermo-mechanical degradation of fingers in a photovoltaic module under thermal cyclic stress conditions. *Sol. Energy* 174, 1044–1052. <http://dx.doi.org/10.1016/j.solener.2018.10.009>, URL <https://www.sciencedirect.com/science/article/pii/S0038092X18309897>.
- Kumar, R., Gupta, R., 2024. Shunts in crystalline silicon PV modules: A comprehensive review of investigation, characterization, and mitigation. *Sol. Energy Mater. Sol. Cells* 277, 113121.
- Kyranaki, N., Smith, A., Yendall, K., Hutt, D.A., Whalley, D.C., Gottschalg, R., Betts, T.R., 2022. Damp-heat induced degradation in photovoltaic modules manufactured with passivated emitter and rear contact solar cells. *Prog. Photovolt., Res. Appl.* 30 (9), 1061–1071. <http://dx.doi.org/10.1002/pip.3556>, URL [arXiv:https://onlinelibrary.wiley.com/doi/pdf/10.1002/pip.3556](https://onlinelibrary.wiley.com/doi/pdf/10.1002/pip.3556).
- Limmanee, A., Udomdanchant, N., Songtrai, S., Kaewniyompanit, S., Sato, Y., Nakaishi, M., Kittisontirak, S., Sriprapha, K., Sakamoto, Y., 2016. Field performance and degradation rates of different types of photovoltaic modules: A case study in thailand. *Renew. Energy* 89, 12–17.
- Lindig, S., Kaaya, I., Weiß, K.-A., Moser, D., Topic, M., 2018. Review of statistical and analytical degradation models for photovoltaic modules and systems as well as related improvements. *IEEE J. Photovolt.* 8 (6), 1773–1786.
- Luo, W., Khoo, Y.S., Hacke, P., Jordan, D., Zhao, L., Ramakrishna, S., Aberle, A.G., Reindl, T., 2018. Analysis of the long-term performance degradation of crystalline silicon photovoltaic modules in tropical climates. *IEEE J. Photovolt.* 9 (1), 266–271.
- Makrides, G., Zinsser, B., Schubert, M., Georgioui, G.E., 2014. Performance loss rate of twelve photovoltaic technologies under field conditions using statistical techniques. *Sol. Energy* 103, 28–42.
- Mathiak, G., Sommer, J., Herrmann, W., Bogdanski, N., Althaus, J., Reil, F., 2016. PV module damages caused by hail impact and non-uniform snow load. In: 32nd European Photovoltaic Solar Energy Conference and Exhibition. pp. 1692–1696.
- Meena, R., Pareek, A., Gupta, R., 2024. A comprehensive review on interfacial degradation in photovoltaic modules. *Renew. Sustain. Energy Rev.* 189, 113944. <http://dx.doi.org/10.1016/j.rser.2023.113944>, URL <https://www.sciencedirect.com/science/article/pii/S136403212300802X>.
- Mikofski, M.A., Kavulak, D.F.J., Okawa, D., Shen, Y.-C., Terao, A., Anderson, M., Caldwell, S., Kim, D., Boitnott, N., Castro, J., Smith, L.A.L., Lacerda, R., Benjamin, D., Hasselbrink, E.F., 2012. Pvlife: An integrated model for predicting PV performance degradation over 25+ years. In: 2012 38th IEEE Photovoltaic Specialists Conference. pp. 001744–001749. <http://dx.doi.org/10.1109/PVSC.2012.6317932>.
- Miller, D.C., Annigoni, E., Ballion, A., Bokria, J.G., Bruckman, L.S., Burns, D.M., Chen, X., Elliott, L., Feng, J., French, R.H., et al., 2015. Degradation in PV encapsulation transmittance: An interlaboratory study towards a climate-specific test. In: 2015 IEEE 42nd Photovoltaic Specialist Conference. PVSC, IEEE, pp. 1–6.
- Mittag, M., Eitner, U., Neff, T., 2017a. Tpedge: progress on cost-efficient and durable edge-sealed PV modules. In: 33rd EUPVSEC. pp. 25–29.
- Mittag, M., Zech, T., Wiese, M., Blasi, D., Ebert, M., Wirth, H., 2017b. Cell-to-module (CTM) analysis for photovoltaic modules with shingled solar cells. In: 2017 IEEE 44th Photovoltaic Specialist Conference. PVSC, pp. 1531–1536. <http://dx.doi.org/10.1109/PVSC.2017.8366260>.
- Norris, K.C., Landzberg, A.H., 1969. Reliability of controlled collapse interconnections. *IBM J. Res. Dev.* 13 (3), 266–271. <http://dx.doi.org/10.1147/rd.133.0266>.
- Ovatt, S., Kern, D., Jordan, D., Johnston, S., Palmiotti, E., Hacke, P., Deline, C., 2024. Bifacial photovoltaic module degradation dynamics. Tech. rep., National Renewable Energy Laboratory (NREL), Golden, CO (United States).
- Öz, A.K., Neven-du Mont, S., Nikitina, V., Romer, P., von Kutzleben, D., Latif, N.A., Forster, J., Wellens, C., Heinrich, M., Neuhaus, D.H., 2025. Pushing the boundaries: Challenges that arise in manufacturing and designing photovoltaic modules for new application areas. *Sol. Energy Mater. Sol. Cells* 291, 113735.
- Peck, D.S., 1986a. Comprehensive model for humidity testing correlation. In: 24th International Reliability Physics Symposium. pp. 44–50. <http://dx.doi.org/10.1109/IRPS.1986.362110>.
- Peck, D.S., 1986b. Comprehensive model for humidity testing correlation. In: 24th International Reliability Physics Symposium. IEEE, pp. 44–50.
- Pingel, S., Frank, O., Winkler, M., Daryan, S., Geipel, T., Hoehne, H., Berghold, J., 2010. Potential induced degradation of solar cells and panels. In: 2010 35th IEEE Photovoltaic Specialists Conference. pp. 002817–002822. <http://dx.doi.org/10.1109/PVSC.2010.5616823>.
- Pingel, S., Janke, S., Frank, O., 2012. Recovery methods for modules affected by potential induced degradation (PID). In: 27th European Photovoltaic Solar Energy Conference and Exhibition. pp. 3379–3383.
- Pintar, A.L., White, C.C., Sung, L.-P., 2020. Bayesian hierarchical models for service-life prediction of polymers. In: *Service Life Prediction of Polymers and Coatings*. Elsevier, pp. 209–231.
- Poddar, S., Rougieux, F., Evans, J.P., Kay, M., Prasad, A.A., Bremner, S.P., 2024. Accelerated degradation of photovoltaic modules under a future warmer climate. *Prog. Photovolt., Res. Appl.*
- Raghuraman, B., Lakshman, V., Kuitche, J., Shisler, W., Tamizhmani, G., Kapoor, H., 2006. An overview of smud's outdoor photovoltaic test program at arizona state university. In: 2006 IEEE 4th World Conference on Photovoltaic Energy Conference, vol. 2, IEEE, pp. 2214–2216.
- Ravindrababu, S., Gebhardt, P., Philipp, D., Ingrid, H., 2023. Modeling the moisture-induced degradation in PV modules with silicon heterojunction cells. In: *Proceedings of the European Photovoltaic Solar Energy Conference and Exhibition, (2023)*. 020276–001–020276–004. <http://dx.doi.org/10.4229/EUPVSEC2023/4A0.8.2>.
- Ren, J., Zhao, W., Shi, J., Yan, Z., Chen, S., Luo, Y., Wang, G., Han, A., Shi, Q., Xia, Z., Fu, H., Zhao, D., Yu, X., Huang, H., Li, R., Zhang, L., Liu, W., Liu, Z., Meng, F., 2024. Predicting the lifetime of HJT modules towards the outdoor real-world environment. *Sol. Energy Mater. Sol. Cells* 272, 112885. <http://dx.doi.org/10.1016/j.solmat.2024.112885>, URL <https://www.sciencedirect.com/science/article/pii/S0927024824001971>.
- Rodríguez-Gallegos, C.D., Bieri, M., Gandhi, O., Singh, J.P., Reindl, T., Panda, S., 2018. Monofacial vs bifacial si-based PV modules: Which one is more cost-effective. *Sol. Energy* 176, 412–438.
- Rubel, F., Brugger, K., Haslinger, K., Auer, I., et al., 2017. The climate of the European alps: Shift of very high resolution Köppen-Geiger climate zones 1800–2100. *Meteorol. Z.* 26 (2), 115–125.
- Schnepf, J., Hummel, S., Lechner, P., 2015. Evaluation of recovery methods after potential induced degradation of PV modules. In: *EU PVSEC 2015*. pp. 1821–1824, URL <https://api.semanticscholar.org/CorpusID:138927920>.
- Schweiger, M., Bonilla, J., Herrmann, W., Gerber, A., Rau, U., 2017. Performance stability of photovoltaic modules in different climates. *Prog. Photovolt., Res. Appl.* 25 (12), 968–981.
- Sharma, V., Sastry, O., Kumar, A., Bora, B., Chandel, S., 2014. Degradation analysis of a-si(HIT) hetero-junction intrinsic thin layer silicon and mc-si solar photovoltaic technologies under outdoor conditions. *Energy* 72, 536–546.
- Sinha, A., Kumar, D., Kempe, M., Jordan, D., Tamizhmani, G., 2018. Activation energy determination for photovoltaic encapsulant discoloration by indoor accelerated UV testing. In: 2018 IEEE 7th World Conference on Photovoltaic Energy Conversion (WCPEC)(a Joint Conference of 45th IEEE PVSC, 28th PVSEC & 34th EU PVSEC). IEEE, pp. 1336–1341.
- Sinha, A., Qian, J., Moffitt, S.L., Hurst, K., Terwilliger, K., Miller, D.C., Schelhas, L.T., Hacke, P., 2023. UV-induced degradation of high-efficiency silicon PV modules with different cell architectures. *Prog. Photovolt., Res. Appl.* 31 (1), 36–51.
- Sinha, A., Sastry, O., Gupta, R., 2016. Nondestructive characterization of encapsulant discoloration effects in crystalline-silicon PV modules. *Sol. Energy Mater. Sol. Cells* 155, 234–242.
- Spataru, S., Hacke, P., Sera, D., 2017. Automatic detection of inactive solar cell cracks in electroluminescence images. In: 2017 IEEE 44th Photovoltaic Specialist Conference. PVSC, pp. 1421–1426. <http://dx.doi.org/10.1109/PVSC.2017.8366106>.
- Spataru, S., Hacke, P., Sera, D., Glick, S., Kerekes, T., Teodorescu, R., 2015. Quantifying solar cell cracks in photovoltaic modules by electroluminescence imaging. In: 2015 IEEE 42nd Photovoltaic Specialist Conference. PVSC, IEEE, pp. 1–6.
- Springer, M., Hartley, J., Bosco, N., 2021. Multiscale modeling of shingled cell photovoltaic modules for reliability assessment of electrically conductive adhesive cell interconnects. *IEEE J. Photovolt.* 11 (4), 1040–1047. <http://dx.doi.org/10.1109/JPHOTOV.2021.3066302>.
- Springer, M., Jordan, D.C., Barnes, T.M., 2023. Future-proofing photovoltaics module reliability through a unifying predictive modeling framework. *Prog. Photovolt., Res. Appl.* 31 (5), 546–553. <http://dx.doi.org/10.1002/pip.3645>, URL [arXiv:https://onlinelibrary.wiley.com/doi/pdf/10.1002/pip.3645](https://onlinelibrary.wiley.com/doi/pdf/10.1002/pip.3645).
- Stein, J., Reise, C., Castro, J.B., Friesen, G., Maugeri, G., Urrejola, E., Ranta, S., 2021. Bifacial photovoltaic modules and systems: Experience and results from international research and pilot applications. Tech. rep., Sandia National Laboratories (SNL-NM), Albuquerque, NM (United States) . . .
- Theristis, M., Stein, J.S., Deline, C., Jordan, D., Robinson, C., Sekulic, W., Anderberg, A., Colvin, D.J., Walters, J., Seigneur, H., et al., 2023. Onymous early-life performance degradation analysis of recent photovoltaic module technologies. *Prog. Photovolt., Res. Appl.* 31 (2), 149–160.
- Thomas, R., Gaines, G., 1979. Methodology for designing accelerated aging tests for predicting life of photovoltaic arrays. In: *NBS/DOE workshop, stability of (thin film) solar cells and materials*, vol. 400, US Department of Commerce, National Bureau of Standards, p. 150.
- Tong, R., Wu, W., Wang, Z., 2024. Factors influencing standard PID test and anti-PID performance of ga-doped PERC mono-facial photovoltaic modules. *J. Electron. Mater.* 1–12.
- Turek, M., Meusel, M., 2023. Automated classification of electroluminescence images using artificial neural networks in correlation to solar cell performance parameters. *Sol. Energy Mater. Sol. Cells* 260, 112483.
- Wald, L., 2018. A simple algorithm for the computation of the spectral distribution of the solar irradiance at surface (Ph.D. thesis). Mines ParisTech.
- Wang, P., Coit, D.W., 2004. Reliability prediction based on degradation modeling for systems with multiple degradation measures. In: *Annual Symposium Reliability and Maintainability, 2004-RAMS*. IEEE, pp. 302–307.
- Wen, Y., Wu, J., Das, D., Tseng, T.-L.B., 2018. Degradation modeling and RUL prediction using Wiener process subject to multiple change points and unit heterogeneity. *Reliab. Eng. Syst. Saf.* 176, 113–124.

- Wenham, S.R., Green, M.A., Watt, M.E., Corkish, R., Sproul, A., 2013. *Applied photovoltaics*. Routledge.
- Wes McKinney, 2010. Data structures for statistical computing in python. In: van der Walt, S., Millman, J. (Eds.), *Proceedings of the 9th Python in Science Conference*. pp. 56–61. <http://dx.doi.org/10.25080/Majora-92bf1922-00a>.
- Witteck, R., Veith-Wolf, B., Schulte-Huxel, H., Morlier, A., Vogt, M.R., Köntges, M., Brendel, R., 2017. UV-induced degradation of PERC solar modules with UV-transparent encapsulation materials. *Prog. Photovolt., Res. Appl.* 25 (6), 409–416.
- Yang, J., Tang, Y., Zhou, C., Chen, S., Cheng, S., Wang, L., Zhou, S., Jia, X., Wang, W., Xu, X., et al., 2024. Unveiling the mechanism of ultraviolet-induced degradation in silicon heterojunction solar cells. *Sol. Energy Mater. Sol. Cells* 276, 113062.
- Zagorowska, M., Wu, O., Ottewill, J.R., Reble, M., Thornhill, N.F., 2020. A survey of models of degradation for control applications. *Annu. Rev. Control.* 50, 150–173. <http://dx.doi.org/10.1016/j.arcontrol.2020.08.002>, URL <https://www.sciencedirect.com/science/article/pii/S1367578820300559>.